Table 1   Characteristics of protein S K196E mutation

Characteristics	Description
Genetic mutation	586A>G in cDNA
	67951A>G in genomic DNA
Amino acid change	Lys-to-Glu (K196E) mutation in the second EGF-like domain
	(Lys155Glu using the nomenclature system of mature protein numbering)
Allele frequency	0.009 in 3,651 Japanese [12]
	0.008 in 183 Japanese [10]
	0.008 in 304 Japanese [48]
Odds ratio (95% confidence interval) to VTE	5.58 (3.11-10.01) [12]
	3.74 (1.06-13.2) [48]
Plasma protein S activity	71.9%±17.6% (mean±SD) in 34 heterozygotes [52]
	(16% lower than the mean of normal individuals)
Detection methods	Method 1: Restriction fragment length polymorphism method using mutagenic primer. Amplify the target 434-bp region by PCR using primer 5'-CAATTTTAGAATTCCATGACATGAGA and mutagenic primer 5'-CCATCCTGCTCTTACCTTTACAATCTGACT. The PCR fragments are digested with Hinf I restriction enzyme. The E-allele gives rise to the 404-bp and 30-bp fragments.[10]
	Method 2: TaqMan genotype discrimination method. PCR primers, 5'-ACCACTGTTCCTGTAAAAATGGTTT, 5'-TGTGTTTTAATTCTACCATCCTGCT. Probes, 5'-VIC-CAAATGAGAAAGATTGTAAAG-MGB (mutant E-allele)/ 5'-FAM-CAAATAAGAAAGATTGTAAAG-MGB (wild-type allele).[52]
Functional study using recombinant protein S E 196-mutant	Molecular weight: same with the wild-type
	Activated protein C does not bind to the mutant.[49]

mutations have not been detected in 47% of protein S-deficient families.[53] The reason for the missing identification of causative mutations in patients with well-characterized protein S deficiency is currently unclear.

This situation might implicate the causative genetic defects in other loci or other genes involved in protein S deficiency.[19] However, cosegregation between certain microsatellite haplotypes and protein S deficiency has been observed in families without any causative mutations in the PROS1 gene, indicating that the causative genetic defects for protein S deficiency are located in or close to the PROS1 gene.[53]

Another explanation for the absence of identified mutations might be mutations in the promoter region or in introns. Transcription of protein S mRNA was directed at multiple start sites,[54] and the PROS1 promoter was shown to contain a forkhead box A2-binding site and an Sp1-binding site.[54] The PROS1 promoter also has liver-specific cis-acting DNA elements for regulation of transcription.[55] Binding sites for various transcription factors within the first 400-bp proximal to the PROS1 translational start codon were further identified, among which only Sp1 and Sp3 play a crucial role in basal expression of the PROS1 gene.[56] A mu-

tation in the PROS1 promoter region responsible for protein S deficiency has been reported in a patient.[57] The C-to-T mutation was within the core binding site of Sp1 and disrupted the Sp1 binding to the promoter, thereby causing reduced PROS1 expression.

Other possible causes of protein S deficiency are the existence of large deletions, duplications, or inversions covering the whole or part of the PROS1 gene, which are difficult to identify by sequencing. They may explain the genetic abnormalities in patients with protein S deficiency.

Large deletions of PROS1 in mutation-negative patients with protein S deficiency

Hereditary thrombophilia associated with protein S deficiency might result from deletion of the PROS1 gene. By now, six large gene deletions have been described in families with protein S deficiency (Table 2).

Using Southern blotting, a patient with protein S deficiency was found to have a deletion of the middle portion of the PROS1 coding sequence.[58] Subsequently, the precise location of the deletion within introns 7 and 11 was identified. This deletion resulted in removal of approximately 14 kb of sequence.[59] The data for this family show for the first time

Table 2   Large gene deletions in PROS1 found in patients with protein S deficiency

Length of deletion	Position of deletion	Analytical methods	Number of PROS1-deficiency families	References
5.3 kb	intron 12 to intron 13	Southern blotting	two	60
14 kb	intron 7 to intron 11	Southern blotting, long PCR	one	59
35 kb	exon 5 to exon 15	SNP and microsatellite markers	one	61
437 kb	exon 1 to exon 11	segregation analysis	one	
449 kb	exon 1 to exon 15		one	
107-729 kb	at least from the promoter to exon 15, at most from centromere to before D3S3619*	MLPA, Q-PCR, microsatellite analysis, SNPs linkage	one	63

*First heterozygous marker in the upstream of PROS1
MLPA : multiplex ligation-dependent probe amplification, Q-PCR: quantitative PCR

the association between protein S deficiency and the gene deletion in PROS1.

A 5.3-kb deletion spanning over 90% of intron 12, all of exon 13, and approximately a quarter of intron 13, was detected in two families with protein S deficiency.[60] This deletion would generate a stop codon at position 463.

In 2005, a highly important study was published regarding the frequency of a large deletion of PROS1 in mutation-negative Swedish patient families with protein S deficiency.[61] Prior to this study, the genetic mutations in PROS1 were first investigated by a PCR-based method in 17 families with protein S deficiency and identified 7 causative mutations in 9 families.[62] The causative mutations in the remaining 8 families were not identified. There was then an attempt to identify the large PROS1 gene deletions in these 8 patients using a dense set of SNP and microsatellite markers in segregation analysis.[61] Finally, gene deletions were identified in 3 out of 8 investigated families. Three deletions encompassed at least 35 kb including exons 5-15, 437 kb including exons 1-11, and 449 kb including the whole PROS1 gene, respectively (Table 2). The last two large deletions included 3 genes, ARL2L1(ARL13B), DHFRL1, and NSUN3, but these deletions were not regarded as the cause of the protein S deficiency. Thus, an important finding of this study is that the frequency of PROS1 gene deletion in PROS1 mutation-negative Swedish VTE patients was 38% (3 out of 9 families). This result translates to an overall frequency of large deletions in patients with protein S deficiency of 18% (3 out of 17 families).

We investigated whether large deletions may exist in PROS1 in Japanese VTE patients. A multiplex ligation-dependent probe amplification (MLPA) analysis was employed to identify the deletion in PROS1 in 163 Japanese patients with VTE.[63] A large gene deletion was identified in only 1 patient who showed 16% protein S activity and did not carry causative point mutations in PROS1 by conventional DNA sequencing (Table 2). The deletion was validated by the quantitative PCR method. The deletion spanned at least the whole PROS1 gene (107 kb) and at most from the cen-

tromere located downstream of PROS1, to before the D3S3619 marker, the first heterozygous marker in the upstream region of PROS1.

As for the frequency of the PROS1 gene deletion, we unfortunately did not measure the protein S activity in all 163 patients with VTE, but measured the activities of protein S and protein C in only 34 patients. Among them, we found 11 patients with protein S deficiency with low protein S activity of less than 50% and with protein C activity of more than 90%. Among these patients, five carried missense or splice site mutations. Among the remaining 6 patients, we found 1 with the PROS1 gene deletion. Therefore, the frequency of the PROS1 gene deletion in PROS1 mutation-negative Japanese VTE patients was estimated to be 17% (1 out of 6 patients). This result translates to an overall frequency of large deletions in patients with protein S deficiency of 9% (1 out of 11 families). Both studies suggested that large deletions are likely to be found in protein S-deficient families where conventional PCR-based mutation screening has failed. Thus, screening for gene deletions in PROS1 might be warranted in PROS1 causative point mutation-negative VTE patients with protein S deficiency.

Perspective on the detection of genomic alterations of PROS1 in protein S deficiency

With a few exceptions, gene dosage measurements are not routine in most mutation scanning studies; alterations of gene dosage on the kb scale are therefore almost certainly under-estimated. As mentioned above, causative mutations in PROS1 could not be identified in approximately half of the cases with protein S deficiency by conventional sequencing of the protein coding region using the PCR-based methods, suggesting the possible existence of undetected genomic aberrations, including duplications, deletions, or inversions, that can involve gain or loss of genetic material of PROS1 in protein S deficiency. In addition, cryptic mutations occurred in introns may generate a new splice acceptor site that disturbs the correct mRNA transcript. In this case, intensive sequencing of the entire

PROS1 gene, including introns, may be needed to identify the cryptic mutations in those patients, and these efforts might uncover the pathogenesis of protein S deficiency.

A wide range of traditional methods, including Southern blotting, long PCR, real-time quantitative PCR, microsatellite and SNP linkage analyses, and MLPA, are useful for gene-dosage measurement, but none offers an overwhelming advantage.[64] An array-based comparative genomic hybridization method containing densely selected large insert DNA fragments distributed roughly every 1 Mb throughout the human genome was developed to detect large-scale copy-number variations that involve gains or losses of several to hundreds of kb of genomic DNA.[65] This method has the potential to perform whole genome scans for altered gene dosage. A molecular copy-number counting method could precisely delineate regions with known or cryptic genomic alterations. Haplotype-fusion PCR followed by bead-based single-molecule haplotyping on repeat-specific markers method could be used for genotyping inversion events with breakpoints embedded within long (>100 kb) inverted repeats.[66] Recently, the high-density array chip technology is available for genome-wide linkage analysis, association, and copy number studies. Those high-density arrays contain more than 1.8 million markers for SNPs and copy number variations. Even though those genome-wide approaches have high throughput, their copy number variation algorisms are indirect because they depend on signal-intensity differences to predict regions of variation. In addition, they cannot detect inversions. Quite recently, intermediate scale structural variations were reported in eight individuals.[67] The methodology utilized in this study appears promising. These types of new methodologies will lead to a more accurate understanding of the extent of both pathogenic and nonpathogenic gene-dosage changes in PROS1 underlying protein S deficiency.

References

1. Dahlback B. Progress in the understanding of the protein C anticoagulant pathway. Int J Hematol 2004;79:109-16.
2. Dahlback B, Villoutreix BO. Regulation of blood coagulation by the protein C anticoagulant pathway: novel insights into structure-function relationships and molecular recognition. Arterioscler Thromb Vasc Biol 2005;25:1311-20.
3. Maurissen LF, Thomassen MC, Nicolaes GA, et al. Re-evaluation of the role of the protein S-C4b binding protein complex in activated protein C-catalyzed factor Va-inactivation. Blood 2008;111:3034-41.
4. Comp PC, Nixon RR, Cooper MR, Esmon CT. Familial protein S deficiency is associated with recurrent thrombosis. J Clin Invest 1984;74:2082-8.
5. Dykes AC, Walker ID, McMahon AD, et al. A study of protein S antigen levels in 3788 healthy volunteers: influence of age, sex and hormone use, and estimate for prevalence of deficiency state. Br J Haematol 2001;113:636-41.
6. Tsuda H, Hattori S, Tanabe S, et al. Screening for aetiology of thrombophilia: a high prevalence of protein S abnormality. Ann Clin Biochem 1999;36 (Pt 4):423-32.
7. Nomura T, Suehisa E, Kawasaki T, Okada A. Frequency of protein S deficiency in general Japanese population. Thromb Res 2000;100:367-71.
8. Suehisa E, Nomura T, Kawasaki T, Kanakura Y. Frequency of natural coagulation inhibitor (antithrombin III, protein C and protein S) deficiencies in Japanese patients with spontaneous deep vein thrombosis. Blood Coagul Fibrinolysis 2001;12:95-9.
9. Sakata T, Okamoto A, Mannami T, et al. Prevalence of protein S deficiency in the Japanese general population: the Suita Study. J Thromb Haemost 2004;2:1012-3.
10. Yamazaki T, Sugiura I, Matsushita T, et al. A phenotypically neutral dimorphism of protein S: the substitution of Lys155 by Glu in the second EGF domain predicted by an A to G base exchange in the gene. Thromb Res 1993;70:395-403.
11. Hayashi T, Nishioka J, Shigekiyo T, et al. Protein S Tokushima: abnormal molecule with a substitution of Glu for Lys-155 in the second epidermal growth factor-like domain of protein S. Blood 1994;83:683-90.
12. Kimura R, Honda S, Kawasaki T, et al. Protein S-K196E mutation as a genetic risk factor for deep vein thrombosis in Japanese patients. Blood 2006;107:1737-8.
13. Miyata T, Kimura R, Kokubo Y, Sakata T. Genetic risk factors for deep vein thrombosis among Japanese: importance of protein S K196E mutation. Int J Hematol 2006;83:217-23.
14. Gandrille S, Borgel D, Sala N, et al. Protein S deficiency: a database of mutations-summary of the first update. Thromb Haemost 2000;84:918.
15. Daly ME, Beauchamp NJ. Inherited protein S deficiency: from genotype to phenotype. Haematologica 2003;88:363-7.
16. Fair DS, Marlar RA, Levin EG. Human endothelial cells synthesize protein S. Blood 1986;67:1168-71.
17. Pan EY, Gomperts ED, Millen R, Gilsanz V. Bone mineral density and its association with inherited protein S deficiency. Thromb Res 1990;58:221-31.
18. Maillard C, Berruyer M, Serre CM, et al. Protein-S, a vitamin K-dependent protein, is a bone matrix component synthesized and secreted by osteoblasts. Endocrinology 1992;130:1599-604.
19. Lane DA, Mannucci PM, Bauer KA, et al. Inherited thrombophilia: Part 1. Thromb Haemost 1996;76:651-62.
20. Dahlback B. The protein C anticoagulant system: inherited defects as basis for venous thrombosis. Thromb Res 1995;77:1-43.
21. Hackeng TM, Sere KM, Tans G, Rosing J. Protein S stimulates inhibition of the tissue factor pathway by tissue factor pathway inhibitor. Proc Natl Acad Sci U S A 2006;103:3106-11.
22. Stitt TN, Conn G, Gore M, et al. The anticoagulation factor protein S and its relative, Gas6, are ligands for the Tyro 3/Axl family of receptor tyrosine kinases. Cell 1995;80:661-70.

23. Webb JH, Blom AM, Dahlback B. Vitamin K-dependent protein S localizing complement regulator C4b-binding protein to the surface of apoptotic cells. J Immunol 2002;169:2580-6.

24. Rezende SM, Simmonds RE, Lane DA. Coagulation, inflammation, and apoptosis: different roles for protein S and the protein S-C4b binding protein complex. Blood 2004;103:1192-201.

25. Garcia de Frutos P, Alim RI, Hardig Y, et al. Differential regulation of alpha and beta chains of C4b-binding protein during acute-phase response resulting in stable plasma levels of free anticoagulant protein S. Blood 1994;84:815-22.

26. Zoller B, Garcia de Frutos P, Dahlback B. Evaluation of the relationship between protein S and C4b-binding protein isoforms in hereditary protein S deficiency demonstrating type I and type III deficiencies to be phenotypic variants of the same genetic disease. Blood 1995;85:3524-31.

27. Simmonds RE, Zoller B, Ireland H, et al. Genetic and phenotypic analysis of a large (122-member) protein S-deficient kindred provides an explanation for the familial coexistence of type I and type III plasma phenotypes. Blood 1997;89:4364-70.

28. Persson KE, Hillarp A, Dahlback B. Analytical considerations for free protein S assays in protein S deficiency. Thromb Haemost 2001;86:1144-7.

29. D'Angelo A, Vigano-D'Angelo S, Esmon CT, Comp PC. Acquired deficiencies of protein S. Protein S activity during oral anticoagulation, in liver disease, and in disseminated intravascular coagulation. J Clin Invest 1988;81:1445-54.

30. Fernandez JA, Estelles A, Gilabert J, et al. Functional and immunologic protein S in normal pregnant women and in full-term newborns. Thromb Haemost 1989;61:474-8.

31. Henkens CM, Bom VJ, Van der Schaaf W, et al. Plasma levels of protein S, protein C, and factor X: effects of sex, hormonal state and age. Thromb Haemost 1995;74:1271-5.

32. Comp PC, Thurnau GR, Welsh J, Esmon CT. Functional and immunologic protein S levels are decreased during pregnancy. Blood 1986;68:881-5.

33. Koster T, Rosendaal FR, Briet E, et al. Protein C deficiency in a controlled series of unselected outpatients: an infrequent but clear risk factor for venous thrombosis (Leiden Thrombophilia Study). Blood 1995;85:2756-61.

34. Faioni EM, Valsecchi C, Palla A, et al. Free protein S deficiency is a risk factor for venous thrombosis. Thromb Haemost 1997; 78:1343-6.

35. Garcia de Frutos P, Fuentes-Prior P, Hurtado B, Sala N. Molecular basis of protein S deficiency. Thromb Haemost 2007;98: 543-56.

36. Martinelli I, Mannucci PM, De Stefano V, et al. Different risks of thrombosis in four coagulation defects associated with inherited thrombophilia: a study of 150 families. Blood 1998;92: 2353-8.

37. Simmonds RE, Ireland H, Lane DA, et al. Clarification of the risk for venous thrombosis associated with hereditary protein S deficiency by investigation of a large kindred with a characterized gene defect. Ann Intern Med 1998;128:8-14.

38. Makris M, Leach M, Beauchamp NJ, et al. Genetic analysis, phenotypic diagnosis, and risk of venous thrombosis in families with inherited deficiencies of protein S. Blood 2000;95: 1935-41.

39. Vossen CY, Conard J, Fontcuberta J, et al. Familial thrombophilia and lifetime risk of venous thrombosis. J Thromb Haemost 2004;2:1526-32.

40. Sacco RL, Owen J, Mohr JP, et al. Free protein S deficiency: a possible association with cerebrovascular occlusion. Stroke 1989; 20:1657-61.

41. Koller H, Stoll G, Sitzer M, et al. Deficiency of both protein C and protein S in a family with ischemic strokes in young adults. Neurology 1994;44:1238-40.

42. Okada H, Yamazaki T, Takagi A, et al. In vitro characterization of missense mutations associated with quantitative protein S deficiency. J Thromb Haemost 2006;4:2003-9.

43. Seligsohn U, Lubetsky A. Genetic susceptibility to venous thrombosis. N Engl J Med 2001;344:1222-31.

44. Beauchamp NJ, Dykes AC, Parikh N, et al. The prevalence of, and molecular defects underlying, inherited protein S deficiency in the general population. Br J Haematol 2004;125:647-54.

45. Bertina RM, Ploos van Amstel HK, van Wijngaarden A, et al. Heerlen polymorphism of protein S, an immunologic polymorphism due to dimorphism of residue 460. Blood 1990;76: 538-48.

46. Espinosa-Parrilla Y, Navarro G, Morell M, et al. Homozygosity for the protein S Heerlen allele is associated with type I PS deficiency in a thrombophilic pedigree with multiple risk factors. Thromb Haemost 2000;83:102-6.

47. Koenen RR, Gomes L, Tans G, et al. The Ser460Pro mutation in recombinant protein S Heerlen does not affect its APC-cofactor and APC-independent anticoagulant activities. Thromb Haemost 2004;91:1105-14.

48. Kinoshita S, Iida H, Inoue S, et al. Protein S and protein C gene mutations in Japanese deep vein thrombosis patients. Clin Biochem 2005;38:908-15.

49. Hayashi T, Nishioka J, Suzuki K. Molecular mechanism of the dysfunction of protein S(Tokushima) (Lys155—>Glu) for the regulation of the blood coagulation system. Biochim Biophys Acta 1995;1272:159-67.

50. Hayashi T, Nishioka J, Suzuki K. Characterization of dysfunctional protein S-Tokushima (K155—>E) in relation to the molecular interactions required for the regulation of blood coagulation. Pol J Pharmacol 1996;48:221-3.

51. Shigekiyo T, Uno Y, Kawauchi S, et al. Protein S Tokushima: an abnormal protein S found in a Japanese family with thrombosis. Thromb Haemost 1993;70:244-6.

52. Kimura R, Sakata T, Kokubo Y, et al. Plasma protein S activity correlates with protein S genotype but is not sensitive to identify K196E mutant carriers. J Thromb Haemost 2006;4:2010-3.

53. Lanke E, Johansson AM, Hillarp A, et al. Co-segregation of the PROS1 locus and protein S deficiency in families having no detectable mutations in PROS1. J Thromb Haemost 2004;2: 1918-23.

54. De Wolf CJ, Cupers RM, Bertina RM, Vos HL. Initiation of protein S mRNA synthesis in human liver and various cell lines. J Thromb Haemost 2005;3:410-2.

55. Tatewaki H, Tsuda H, Kanaji T, et al. Characterization of the human protein S gene promoter: a possible role of transcription factors Sp1 and HNF3 in liver. Thromb Haemost 2003; 90:1029-39.

56. de Wolf CJ, Cupers RM, Bertina RM, Vos HL. The constitutive expression of anticoagulant protein S is regulated through multiple binding sites for Sp1 and Sp3 transcription factors in the protein S gene promoter. J Biol Chem 2006;281:17635-43.

57. Sanda N, Fujimori Y, Kashiwagi T, et al. An Sp1 binding site mutation of the PROS1 promoter in a patient with protein S

deficiency. Br J Haematol 2007;138:663-5.

58. Ploos van Amstel HK, Huisman MV, Reitsma PH, et al. Partial protein S gene deletion in a family with hereditary thrombophilia. Blood 1989;73:479-83.

59. Holmes ZR, Bertina RM, Reitsma PH. Characterization of a large chromosomal deletion in the PROS1 gene of a patient with protein S deficiency type I using long PCR. Br J Haematol 1996;92:986-91.

60. Schmidel DK, Nelson RM, Broxson EH, Jr., et al. A 5.3-kb deletion including exon XIII of the protein S alpha gene occurs in two protein S-deficient families. Blood 1991;77:551-9.

61. Johansson AM, Hillarp A, Sall T, et al. Large deletions of the PROS1 gene in a large fraction of mutation-negative patients with protein S deficiency. Thromb Haemost 2005;94:951-7.

62. Rezende SM, Lane DA, Zoller B, et al. Genetic and phenotypic variability between families with hereditary protein S deficiency.

Thromb Haemost 2002;87:258-65.

63. Yin T, Takeshita S, Sato Y, et al. A large deletion of the PROS1 gene in a deep vein thrombosis patient with protein S deficiency. Thromb Haemost 2007;98:783-9.

64. Armour JA, Barton DE, Cockburn DJ, Taylor GR. The detection of large deletions or duplications in genomic DNA. Hum Mutat 2002;20:325-37.

65. Iafrate AJ, Feuk L, Rivera MN, et al. Detection of large-scale variation in the human genome. Nat Genet 2004;36:949-51.

66. Turner DJ, Shendure J, Porreca G, et al. Assaying chromosomal inversions by single-molecule haplotyping. Nat Methods 2006; 3:439-45.

67. Kidd JM, Cooper GM, Donahue WF, et al. Mapping and sequencing of structural variation from eight human genomes. Nature 2008;453:56-64.

The distal carboxyl-terminal domains of ADAMTS13 are required for regulation of in vivo thrombus formation

Fumiaki Banno,[1] Anil K. Chauhan,[2,3] Koichi Kokame,[1] Jin Yang,[1] Shigeki Miyata,[4] Denisa D. Wagner,[2,3] and Toshiyuki Miyata[1]

[1]Research Institute, National Cardiovascular Center, Suita, Japan; [2]Immune Disease Institute and [3]Department of Pathology, Harvard Medical School, Boston, MA; and [4]Division of Transfusion Medicine, National Cardiovascular Center, Suita, Japan

ADAMTS13 is a multidomain protease that limits platelet thrombogenesis through the cleavage of von Willebrand factor (VWF). We previously identified 2 types of mouse Adamts13 gene: the 129/Sv-strain Adamts13 gene encodes the long-form ADAMTS13 having the same domains as human ADAMTS13, whereas the C57BL/6-strain Adamts13 gene encodes the short-form ADAMTS13 lacking the distal C-terminal domains. To assess the physiologic significance of the distal C-terminal domains of ADAMTS13, we generated and analyzed 129/Sv-genetic background congenic mice (Adamts13$^{S/S}$) that carry the short-form ADAMTS13. Similar to wild-type 129/Sv mice (Adamts13$^{L/L}$), Adamts13$^{S/S}$ did not have ultralarge VWF multimers in plasma, in contrast to 129/Sv-genetic background ADAMTS13-deficient mice (Adamts13$^{-/-}$). However, in vitro thrombogenesis under flow at a shear rate of 5000 s^{-1} was accelerated in Adamts13$^{S/S}$ compared with Adamts13$^{L/L}$. Both in vivo thrombus formation in ferric chloride–injured arterioles and thrombocytopenia induced by collagen plus epinephrine challenge were more dramatic in Adamts13$^{S/S}$ than in Adamts13$^{L/L}$ but less than in Adamts13$^{-/-}$. These results suggested that the C-terminally truncated ADAMTS13 exhibited decreased activity in the cleavage of VWF under high shear rate. Role of the C-terminal domains may become increasingly important under prothrombotic conditions. (Blood. 2009;113:5323-5329)

Introduction

ADAMTS13 is a plasma protease that specifically cleaves von Willebrand factor (VWF).[1] VWF is a multimeric plasma glycoprotein that plays a critical role in platelet adhesion and aggregation on vascular lesions.[2] Endothelial cells and megakaryocytes produce mainly VWF as large multimers that can exceed 20 000 kDa in mass and secrete the multimers into the circulating blood. The adhesive activity of VWF multimers depends on their molecular sizes and in particular the largest multimers, called ultralarge VWF (UL-VWF) multimers, can induce excessive platelet aggregation under shear stress. UL-VWF multimers are normally cleaved by ADAMTS13 to smaller forms, thus restraining platelet thrombus formation. The lack of ADAMTS13 activity allows UL-VWF multimers to persist in the circulation and leads to the development of thrombotic thrombocytopenic purpura (TTP).[3-5]

ADAMTS13 consists of multiple domains including a metalloprotease domain, a disintegrin-like domain, a thrombospondin type 1 motif (Tsp1) domain, a cysteine-rich domain, a spacer domain, 7 additional Tsp1 domains and 2 complement components C1r/C1s, urchin epidermal growth factor, and bone morphogenic protein-1 (CUB) domains in order from the N-terminus. So far, the functional roles of ADAMTS13 domains have been studied using in vitro assay systems.[6-13] These studies have shown an essential role of the N-terminal region of ADAMTS13 from the metalloprotease domain to the spacer domain, on the VWF cleavage. However, the results from in vitro studies have lacked consistency on the relative importance of the C-terminal Tsp1 and CUB domains in the substrate recognition and the activity of ADAMTS13. The recombinant human ADAMTS13 mutant lacking the C-terminal

Tsp1 and CUB domains maintain almost absolute VWF-cleaving activity under static conditions, indicating that the C-terminal domains are dispensable for the ADAMTS13 activity.[6-8] Under flow, the same mutant is hyperactive for the cleavage of newly released VWF multimers anchored on endothelial cells, suggesting that the C-terminal domains negatively regulate the activity of ADAMTS13.[10] Recombinant polypeptides and synthetic peptides derived from the first CUB domain can inhibit the cleavage of VWF multimers on endothelial cells by ADAMTS13 under flow.[11] Removal of the C-terminal Tsp1 and CUB domains results in a marked decrease in VWF cleavage by ADAMTS13 in a vortex mixer and in VWF binding to ADAMTS13 in a Biacore system (Uppsala, Sweden),[13] indicating that the C-terminal domains play a crucial role in the recognition and cleavage of VWF. These results prompted us to investigate the role of C-terminal domains of ADAMTS13 in vivo.

In laboratory mouse strains, 2 kinds of Adamts13 gene are present.[14-16] The Adamts13 gene of the 129/Sv strain contains 29 exons like the human ADAMTS13 gene and encodes the full-length ADAMTS13 with the same domain constitutions as human ADAMTS13. On the other hand, several strains of mice, including the C57BL/6 strain, harbor the insertion of an intracisternal A-particle (IAP) retrotransposon into intron 23 of the Adamts13 gene. As a result, the distal C-terminally truncated ADAMTS13 lacking the C-terminal 2 Tsp1 domains and 2 CUB domains is predominantly expressed in these strains. Therefore, mice can be suitable animal models for evaluating functions of the distal C-terminal domains, the C-terminal 2 Tsp1 domains, and 2 CUB domains, in vivo.

In the present study, through using the spontaneous IAP insertion in mouse *Adamts13* gene, we generated a congenic mouse model that had the distal C-terminally truncated ADAMTS13 on 129/Sv genetic background. While comparing with wild-type 129/Sv mice having full-length ADAMTS13 and ADAMTS13-deficient mice on the same genetic background, we analyzed platelet thrombus formation in the congenic mice to define physiologic significance of the distal C-terminal domains in ADAMTS13 functions. Our results indicate that the distal C-terminal domains of ADAMTS13 contribute to the processing of VWF multimers in vivo, and that the importance of these domains becomes obvious after suffering thrombogenic stimuli.

Methods

Animals

The 129/Sv mice were purchased from Clea Japan (Tokyo, Japan). C57BL/6 mice were purchased from Japan SLC (Hamamatsu, Japan). ADAMTS13-deficient mice on the 129/Sv genetic background were described previously.[17,18] ADAMTS13-congenic mice were developed by introgressing the C57BL/6-*Adamts13* gene onto the 129/Sv genetic background, as follows. C57BL/6 mice were backcrossed to 129/Sv mice for 10 generations while retaining the C57BL/6-*Adamts13* gene. In the resulting N10 heterozygous mice, autosomal chromosomes were theoretically 99.9% identical to those of the 129/Sv strain and sex chromosomes were derived exclusively from the 129/Sv strain. The N10 heterozygous mice were interbred to produce homozygous mice. The *Adamts13*-genotype was determined by polymerase chain reaction (PCR) with HotStarTaq DNA polymerase (QIAGEN, Hilden, Germany). The amplification was carried out using primers: the intron 23-specific forward primer, 5'-ACCTCTCAAGT-GTTTGGGATGCTA-3', the IAP-specific reverse primer, 5'-TCAGCGC-CATCTTGTGACGGCGAA-3', and the primer downstream of the IAP target site, 5'-TGCCAGATGGCCATGATTAACTCT-3'. For the experiments, all animals were matched for age and sex. All animal procedures were approved by the Animal Care and Use Committees of the National Cardiovascular Center Research Institute and Immune Disease Institute.

Northern blot analysis

Total RNA was extracted from liver using ISOGEN reagent (Nippon Gene, Tokyo, Japan) and poly(A)$^+$ RNA was purified using PolyATtract mRNA Isolation Systems (Promega, Madison, WI). The alkaline phosphatase–labeled probe was synthesized from mouse *Adamts13* cDNA (1.3 kb) using AlkPhos Direct labeling module (GE Healthcare, Little Chalfont, United Kingdom). Poly(A)$^+$ RNA was separated on a 1% agarose gel containing 2% formaldehyde and transferred to a nylon membrane. The probe was hybridized to the blot and detected using CDP-Star detection reagent (GE Healthcare).

Blood sampling

Blood was collected from the retro-orbital plexus into tubes containing a 0.1 volume of 3.8% sodium citrate. Blood cell counts and hematocrit were determined using an automatic cell counter (KX-21NV; Sysmex, Kobe, Japan). Plasma was prepared from blood by centrifugation at 800g for 15 minutes.

Determination of plasma ADAMTS13 activity

Plasma ADAMTS13 activity was measured using GST-mVWF73-H, a recombinant mouse VWF73 peptide flanked by N-terminal glutathione S-transferase (GST) and C-terminal His$_6$ tags, as described previously.[14] In brief, GST-mVWF73-H (500 ng) was incubated with 0.8 μL plasma in 40 μL reaction buffer (10 mM *N*-2-hydroxyethylpiperazine-*N'*-2-ethanesul-fonic acid, 150 mM NaCl, 5 mM CaCl$_2$, and 0.005% Tween 20, pH 7.4) at 37°C for 1 hour. The reaction was stopped by adding 10 μL sodium dodecyl

sulfate (SDS) sample buffer (50 mM tris(hydeoxymethyl)aminomethane-HCl, 10 mM EDTA, 10% SDS, 250 mM dithiothreitol, 30% glycerol, and 0.1% bromophenol blue, pH 6.8). The samples were subjected to SDS–polyacrylamide gel electrophoresis and Western blot using a rabbit anti-GST antibody (Invitrogen, Carlsbad, CA) and a peroxidase-labeled anti–rabbit IgG antibody (KPL, Gaithersburg, MD). Activity was also determined using a fluorogenic human VWF73 peptide of FRETS-VWF73 (Peptide Institute, Minoh, Japan).[19,20] FRETS-VWF73 (2 μM) was incubated with 4 μL plasma in 200 μL assay buffer (5 mM bis(2-hydroxyethyl)-amino-tris(hydeoxymethyl)methane, 25 mM CaCl$_2$, and 0.005% Tween 20, pH 6.0) at 30°C. Increases in fluorescence were measured using a 350-nm excitation filter and a 440-nm emission filter in a fluorescence photometer (Mx3000P; Stratagene, La Jolla, CA).

VWF multimer analysis

Plasma VWF multimer patterns were analyzed as described previously.[17] Plasma samples in SDS sample buffer were electrophoresed on a 1% agarose gel (Agarose IEF; GE Healthcare) at a constant current of 15 mA at 4°C. After transfer to a nitrocellulose membrane, the membrane was incubated in peroxidase-conjugated rabbit anti–human VWF (1:500; Dako, Glostrup, Denmark) in 5% skim milk to detect VWF multimers. Bound antibody was detected with Western Lighting Chemiluminescence Reagent Plus (PerkinElmer, Waltham, MA) on an image analyzer (LAS-3000; Fujifilm, Tokyo, Japan). The chemiluminescent intensities of each lane were scanned using Image Gauge software (version 4.2.2; Fujifilm); the relative intensity profiles were shown.

Parallel plate flow chamber assay

Platelet thrombus formation in flowing blood on immobilized collagen was analyzed using a parallel plate flow chamber as described previously.[17,21] Acid-insoluble type I collagen–coated glass coverslips were placed in a flow chamber. The chamber was mounted on a fluorescence microscope (Axiovert 200M; Carl Zeiss, Oberkochen, Germany) equipped with a CCD camera system (DXC-390; Sony, Tokyo, Japan). Blood was collected into tubes containing argatroban (240 μM; Mitsubishi Chemical, Tokyo, Japan). The fluorescent dye mepacrine (10 μM; Sigma-Aldrich, St Louis, MO) was added to the blood. Whole blood samples were aspirated through the chamber and across the collagen-coated coverslip at a constant wall shear rate. To analyze the cumulative thrombus volume, image sets at 1.0-μm z-axis intervals within a defined area (156.4 μm × 119.6 μm) were captured using MetaMorph software (version 6.1.4; Universal Imaging, West Chester, PA). After blind deconvolution of image sets processed by AutoDeblur software package (version 8.0.2; AutoQuant Imaging, Troy, NY), 3D volumetric measurements of thrombi were accomplished using VoxBlast software (version 3.0; Vartek, Fairfield, IA).

Intravital microscopy

Intravital microscopy was performed as described previously.[22,23] Platelets were isolated from platelet-rich plasma and fluorescently labeled with calcein AM (2.5 μg/mL; Invitrogen). Recipient mice were anesthetized and labeled platelets were infused through retro-orbital plexus. The mesentery was gently exteriorized through a midline abdominal incision and arterioles of 100- to 150-μm diameters were visualized with a fluorescence microscope and a CCD camera system. The shear rate was calculated using an optical Doppler velocimeter as described.[24] Filter paper saturated with 10% ferric chloride was applied for 5 minutes on an arteriole by topical application. Thrombus formation in the arteriole was monitored for 40 minutes after injury or until complete occlusion occurred and lasted for more than 30 seconds. The following 2 parameters were evaluated: time to first thrombus formation, defined as the time required for formation of a thrombus larger than 30 μm, and occlusion time, defined as the time required for cessation of blood flow for at least 30 seconds.

Collagen plus epinephrine–induced thrombosis model

A mixture of 600 ng/g collagen (Nycomed, Roskilde, Denmark) and 60 ng/g epinephrine (Sigma-Aldrich) was infused into tail vein of mice.[17,25]

Blood was collected 5 minutes after the infusion and platelet counts were determined.

Statistical analysis

Statistical significance was assessed by the one-way analysis of variance followed by the Bonferroni multiple comparison tests. Differences were considered to be significant at P values less than .05.

Results

Generation of Adamts13$^{S/S}$ mice

To address the functional implication of the distal C-terminal domains of ADAMTS13 in vivo, we generated and characterized a congenic mouse model that has the C-terminally truncated form of ADAMTS13 on 129/Sv genetic background (Figure 1A). We confirmed the presence of IAP insertion in the Adamts13 gene of the congenic (Adamts13$^{S/S}$) mice by PCR (data not shown) and detected an IAP chimeric transcript (~ 3.5 kb) by Northern blotting of RNA from liver (Figure 1B), primary site of synthesis.[14] An IAP-free ADAMTS13 mRNA (~ 5 kb) was detected in wild-type 129/Sv (Adamts13$^{L/L}$) mice and no ADAMTS13 mRNA was detected in ADAMTS13-deficient (Adamts13$^{-/-}$) mice on 129/Sv genetic background (Figure 1B). Adamts13$^{S/S}$ mouse plasma exhibited higher cleaving activity for both GST-mVWF73-H and FRETS-VWF73 than Adamts13$^{L/L}$ mouse plasma, whereas the activity in Adamts13$^{-/-}$ mouse plasma was below detection limits (Figure 1C,D). Therefore, the distal C-terminal domains of ADAMTS13 were not necessary for the cleavage of the VWF73-based peptide substrate as observed previously.[8,14] Platelet counts were not different among the genotypes (Adamts13$^{L/L}$, 744 ± 180 × 10^9/L; Adamts13$^{S/S}$, 693 ± 44 × 10^9/L; Adamts13$^{-/-}$, 672 ± 39 × 10^9/L; mean ± SD, n = 8). Both Adamts13$^{S/S}$ mice and Adamts13$^{-/-}$ mice were viable and showed no TTP-like symptoms throughout the study.

Adamts13$^{S/S}$ mice have normal VWF multimers

As previously reported,[17] UL-VWF multimers persisted in plasma of Adamts13$^{-/-}$ mice on 129/Sv-genetic background (Figure 2). Thus, ADAMTS13 activity is important for the size regulation of VWF multimers in mice at least on this genetic background. However, the VWF multimer patterns in Adamts13$^{S/S}$ mice were indistinguishable from those in Adamts13$^{L/L}$ mice (Figure 2). These results suggest that the distal C-terminally truncated form of mouse ADAMTS13 exhibits VWF-cleaving activity sufficient for maintenance of normal size distribution of plasma VWF multimers under steady state in vivo.

In vitro thrombogenesis is increased in Adamts13$^{S/S}$ mice only at a high shear rate

When whole blood was perfused over a collagen-coated surface in a parallel plate flow chamber at a shear rate of 1000 s^{-1}, platelet thrombus formation was significantly promoted in Adamts13$^{-/-}$ mice (Figure 3A) compared with Adamts13$^{L/L}$ mice, consistent with the presence of UL-VWF multimers in plasma of Adamts13$^{-/-}$ mice. However, whole blood thrombus formation at 1000 s^{-1} was not significantly different between Adamts13$^{S/S}$ mice and Adamts13$^{L/L}$ mice (Figure 3A), indicating that the distal C-terminally truncated form of mouse ADAMTS13 does not completely lose the activity.

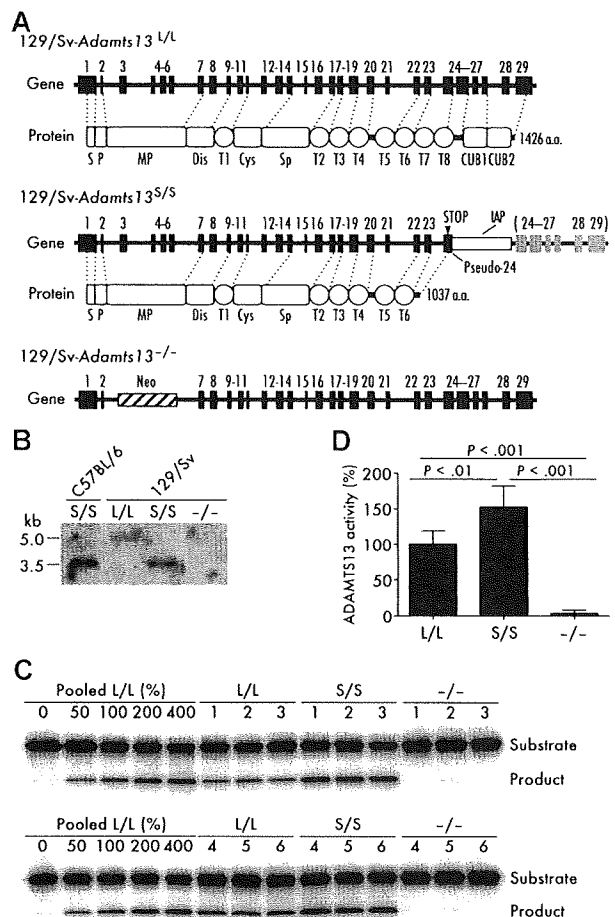As fluid shear rate increases progressively, the interaction between VWF and platelet GPIbα becomes more important in

Figure 1. Generation of Adamts13$^{S/S}$ mice with 129/Sv-genetic background. (A) Gene and protein structure of ADAMTS13 in the wild-type (Adamts13$^{L/L}$) 129/Sv mice, the Adamts13$^{S/S}$ mice on 129/Sv genetic background, and the Adamts13$^{-/-}$ mice on 129/Sv genetic background. An intracisternal A-particle (IAP) insertion into intron 23 creates a pseudo-exon 24 including a premature stop codon. ADAMTS13 with a truncated C-terminus is expressed mainly in Adamts13$^{S/S}$ mice. S indicates signal peptide; P, propeptide; MP, metalloprotease domain; Dis, disintegrin-like domain; T (numbered 1-8), thrombospondin type 1 motif domain; Cys, cysteine-rich domain; Sp, spacer domain; and CUB, complement components C1r/C1s, urchin epidermal growth factor, and bone morphogenic protein-1 domain. (B) Expression of Adamts13 mRNA in liver. Poly(A)$^+$ RNA isolated from liver of indicated mice was probed with a 1.3-kb Adamts13 cDNA corresponding to exons 3 to 13. (C) GST-mVWF73-H assay. Plasma ADAMTS13 activity of indicated mice was measured using a recombinant mouse VWF73 peptide, GST-mVWF73-H. Results from 6 mice for each genotype are shown. Standard reactions using graded amounts of pooled plasma from 10 Adamts13$^{L/L}$ mice were performed simultaneously. (D) FRETS-VWF73 assay. Plasma ADAMTS13 activity in indicated mice was determined using a fluorogenic human VWF73 peptide, FRETS-VWF73. Data are mean ± SD of 6 mice for each genotype. The average activity measured in Adamts13$^{L/L}$ mice was arbitrarily defined as 100%.

platelet thrombus formation.[26] It has been reported that thrombus formation in mouse blood on collagen surface is completely dependent on the VWF-GPIbα interaction above a threshold shear rate between 2000 s^{-1} and 5000 s^{-1}.[27] In addition, ADAMTS13 cleaves VWF and down-regulates thrombus formation in shear rate–dependent manner.[28] Based on these observations, we further examined thrombus formation at a higher shear rate of 5000 s^{-1}. As expected, thrombus formation in Adamts13$^{-/-}$ mice was significantly elevated compared with Adamts13$^{L/L}$ mice at 5000 s^{-1} (Figure 3B). In addition, we found accelerated thrombus formation in Adamts13$^{S/S}$ mice compared with Adamts13$^{L/L}$ mice at this higher shear rate (Figure 3B). These results suggest that the distal C-terminally truncated form of mouse ADAMTS13 has reduced
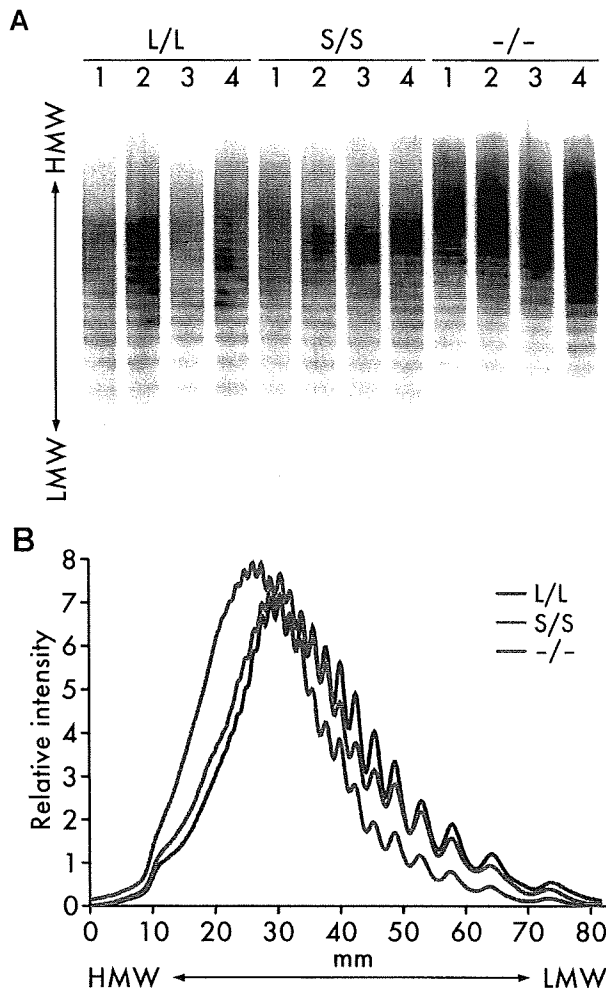
A

B

Figure 2. Plasma VWF multimers. (A) VWF multimer patterns. Plasma samples (1 μL/lane) from Adamts13$^{L/L}$, Adamts13$^{S/S}$, and Adamts13$^{-/-}$ mice were electrophoresed on SDS-agarose gels and transferred to nitrocellulose membranes. VWF multimers were detected with anti-VWF antibodies. (B) Relative intensities of plasma VWF multimers. The chemiluminescent intensities of the VWF multimer patterns (A) were scanned using image analysis software. An average of multiple lanes from 4 mice for each genotype is shown. HMW indicates high molecular weight; LMW, low molecular weight.

activity compared with the full-length form and does not sufficiently limit thrombus formation under high shear rate in vitro.

In vivo thrombus growth is accelerated in Adamts13$^{S/S}$ mice

To examine whether the truncation of the distal C-terminal domains in ADAMTS13 affects thrombus formation in vivo, we carried out intravital microscopy experiments in a model of experimental arteriolar thrombosis. In this model, vascular injury was induced by topical application of ferric chloride on a mesenteric arteriole, which provoked the generation of free radicals leading to the endothelial disruption.[23] The diameter and shear rate of studied arterioles were 118.0 plus or minus 13.1 μm and 1362 plus or minus 219 s^{-1} (mean ± SD, n = 16) for Adamts13$^{L/L}$ mice, 122.8 plus or minus 11.1 μm and 1394 plus or minus 136 s^{-1} (n = 16) for Adamts13$^{S/S}$ mice, and 115.6 plus or minus 10.8 μm and 1405 plus or minus 225 s^{-1} (n = 12) for Adamts13$^{-/-}$ mice and not significantly different among the groups. Both time to first thrombus (Figure 4A) and occlusion time (Figure 4B) after injury in Adamts13$^{-/-}$ mice (time to first thrombus = 5.1 ± 1.9 minutes, occlusion time = 9.2 ± 1.6 minutes; mean ± SD) were signifi-
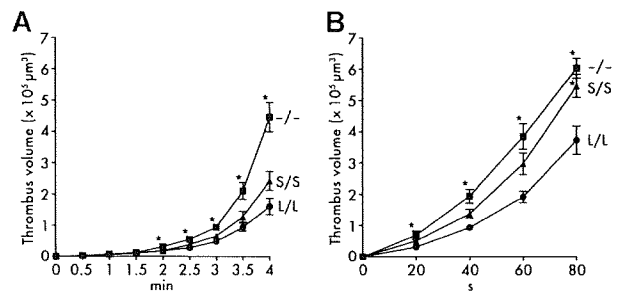
A

B

Figure 3. In vitro thrombogenesis on collagen surface under flow. (A) Thrombus formation at 1000 s^{-1}. Whole blood from Adamts13$^{L/L}$, Adamts13$^{S/S}$, or Adamts13$^{-/-}$ mice containing mepacrine-labeled platelets was perfused over an acid-insoluble type I collagen–coated surface at a wall shear rate of 1000 s^{-1}. The cumulative thrombus volume, analyzed using a multidimensional imaging system, was measured every 0.5 minutes until 4 minutes. Data are the mean ± SEM of 25 mice for each genotype. (B) Thrombus formation at 5000 s^{-1}. Whole-blood samples from indicated mice were perfused over an acid-insoluble type I collagen–coated surface at a wall shear rate of 5000 s^{-1}. The cumulative thrombus volume was measured every 20 seconds until 80 seconds. Blood from 2 mice was pooled and used for experiments. Data are the mean ± SEM of 15 samples for each genotype. *P < .05 in comparison with Adamts13$^{L/L}$ mice.

cantly decreased compared with Adamts13$^{L/L}$ mice (time to first thrombus = 7.8 ± 1.3 minutes, occlusion time = 15.3 ± 3.6 minutes), indicating that ADAMTS13 contributes to down-regulation of thrombogenesis at the site of arteriolar injury in 129/Sv mice. In the case of Adamts13$^{S/S}$ mice, time to first thrombus after injury (7.6 ± 1.2 minutes) was not different from Adamts13$^{L/L}$ mice. However, the initial thrombi grew rapidly to occlusive size in Adamts13$^{S/S}$ mice and occlusion time was significantly shorter in Adamts13$^{S/S}$ mice (12.5 ± 1.9 minutes) compared with Adamts13$^{L/L}$ mice (Figure 4B). These results suggest that the distal C-terminally truncated form of mouse ADAMTS13 is less active in down-regulating thrombus growth in vivo compared with full-length ADAMTS13.

To elucidate the consequences of the lack of the distal C-terminal domains in ADAMTS13 on systemic thrombosis, we performed collagen plus epinephrine infusion model experiments. In this model, widespread intravascular thrombosis was induced by intravenous infusion of collagen fibrils in combination with epinephrine, and the incorporation of platelets into thrombi was monitored by the reduction in circulating platelet counts.[29] Consistent with our previous observation,[17] platelet counts after the infusion were significantly lower in Adamts13$^{-/-}$ mice
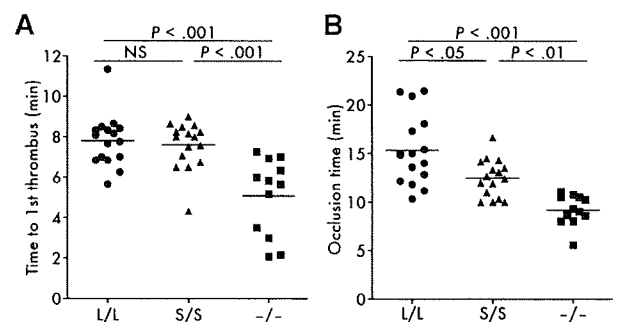
A

B

Figure 4. In vivo thrombogenesis in ferric chloride–injured mesenteric arterioles. (A) Time to first thrombus formation. Calcein AM–labeled platelets representing approximately 2.5% of total platelets were observed in mesenteric arterioles of live mice after injury with 10% ferric chloride. The time required for formation of a thrombus more than 30 μm was measured. (B) Occlusion time. The time required for a complete stop of blood flow was measured after injury with 10% ferric chloride. Symbols represent data from a single mouse. Bars represent the mean values of groups (n = 16 for Adamts13$^{L/L}$ mice, n = 16 for Adamts13$^{S/S}$ mice, and n = 12 for Adamts13$^{-/-}$ mice).
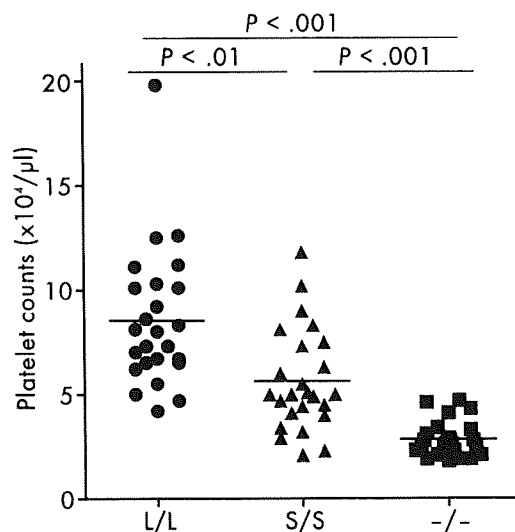
Figure 5. Platelet counts after collagen plus epinephrine infusion. Mice were injected with 600 ng/g collagen plus 60 ng/g epinephrine via tail vein and platelet counts were measured 5 minutes after injection. Symbols represent platelet counts from a single mouse. Bars represent the mean values of 25 mice in each group. Platelet counts of untreated mice were not different among the groups.

(28 ± 8 × 10^9/L, mean ± SD) than in $Adamts13^{L/L}$ mice (85 ± 33 × 10^9/L), suggesting that ADAMTS13 contributes to inhibition of platelet aggregation in this experimental system (Figure 5). Platelet counts after the infusion in $Adamts13^{S/S}$ mice (56 ± 24 × 10^9/L) were significantly higher than in $Adamts13^{-/-}$ mice and lower than in $Adamts13^{L/L}$ mice (Figure 5), whereas platelet counts of untreated mice were not different among the groups ($Adamts13^{L/L}$, 666 ± 44 × 10^9/L; $Adamts13^{S/S}$, 770 ± 65 × 10^9/L; $Adamts13^{-/-}$, 710 ± 49 × 10^9/L, mean ± SD of 4 mice). These findings complement accelerated thrombus growth in $Adamts13^{S/S}$ mice compared with $Adamts13^{L/L}$ mice, indicating that the distal C-terminally truncated form of mouse ADAMTS13 has significantly reduced activity in vivo.

Discussion

It is now evident that genetic background is an important phenotypic determinant in mutant mice with hemostatic defects. For instance, mice carrying the factor V Leiden (R504Q) mutation have shown increased perinatal thrombotic mortality on the mixed 129/Sv and C57BL/6J background relative to C57BL/6J background.[30] Similar effects of genetic backgrounds on phenotypes have been observed in other mutants such as the thrombomodulin G404P-mutant mice,[31] the fibrinogen-deficient mice,[32] and the tissue factor–deficient mice.[33] In ADAMTS13-deficient mice, genetic backgrounds have also been shown to significantly affect their thrombotic phenotypes.[34] Thus, phenotypes of ADAMTS13 mutant mice should be compared with control mice on the appropriate and uniform strain background. We have previously demonstrated that ADAMTS13 deficiency in mice results in a prothrombotic state with accumulation of UL-VWF multimers on 129/Sv background.[17] Therefore in this study, we applied a spontaneous mutation in the $Adamts13$ gene of C57BL/6 mice onto 129/Sv mice by 10-generation backcrossing, and obtained the congenic mice that were expected to have 99.9% 129/Sv genome and primarily expressed the distal C-terminally truncated ADAMTS13. Then, we compared their phenotypes with positive and negative control animals: the wild-type 129/Sv mice and the

129/Sv-background ADAMTS13-deficient mice. By this approach, we minimized the background effects and defined the significance of the distal C-terminal domains of ADAMTS13 in mice.

Plasma of the congenic mice exhibited higher cleaving activity against GST-mVWF73-H and FRETS-VWF73 compared with plasma of the wild-type mice. We previously observed that the recombinant distal C-terminally truncated mouse ADAMTS13 cleaves GST-mVWF73-H to a similar extent compared with the full-length form.[14] The other group reported that the recombinant distal C-terminally truncated mouse ADAMTS13 is slightly less active in cleaving GST-mVWF73-H than the full-length form.[15] These findings suggest that the distal C-terminally truncated ADAMTS13 in mouse plasma has equivalent or slightly lower specific activity against VWF73-based substrates compared with the full-length ADAMTS13. Thus, the data in the present study imply that the distal C-terminally truncated ADAMTS13 is more abundant than the full-length form in circulating blood in 129/Sv mice. Preferential expression of the distal C-terminally truncated mouse ADAMTS13 has also been found in HeLa cells[14] and HEK 293T cells.[15] Unfortunately, because we have failed to determine the ADAMTS13 antigen levels in mouse plasma, it remains unclear whether the distal C-terminal truncation of ADAMTS13 actually increases plasma levels of the enzyme. Despite the congenic mice having higher in vitro ADAMTS13 activity in plasma, they showed prothrombotic phenotypes, suggesting the importance of the distal C-terminal domains in ADAMTS13 activity in vivo.

We reconfirmed that ADAMTS13 deficiency in 129/Sv mice allowed the accumulation of UL-VWF multimers in plasma (Figure 2), therefore, promising the essential contribution of ADAMTS13 on preventing the accumulation of UL-VWF multimers in 129/Sv mice. Under these situations, lack of the distal C-terminal domains of ADAMTS13 in 129/Sv mice did not increase plasma VWF multimer sizes (Figure 2), showing that the distal C-terminally truncated ADAMTS13 maintained the VWF-cleaving activity in vivo. Although the distal C-terminally truncated form of mouse ADAMTS13 was reported to show considerably lower activity than the full-length form for purified human VWF multimers under in vitro static conditions,[15] our results show that the distal C-terminal truncation of mouse ADAMTS13 allows retention of normal size distribution of plasma VWF multimers in vivo at least under steady state.

In the parallel-plate flow chamber experiments, ADAMTS13 deficiency in 129/Sv mice markedly enhanced thrombogenic responses (Figure 3), indicating that ADAMTS13 is critical for limiting platelet thrombus formation under whole blood flow conditions. In the same experimental conditions, the distal C-terminal truncation of ADAMTS13 in 129/Sv mice did not promote thrombogenesis at 1000 s^{-1} (Figure 3A) but significantly promoted thrombogenesis at 5000 s^{-1} (Figure 3B). It is conceivable that the distal C-terminally truncated ADAMTS13 is active but not fully competent to cleave VWF within growing thrombus under flow. Because both the interaction of GPIbα-VWF and the cleavage of VWF by ADAMTS13 are facilitated by increasing fluid shear rate, the function of the distal C-terminal domains may become vital to down-regulate thrombogenesis under high shear conditions. Actually, similar results were obtained in the in vivo arteriolar injury model experiments (Figure 4). The distal C-terminal truncation of ADAMTS13 in 129/Sv mice did not affect the time to first thrombus formation in the arterioles where fluid shear rates were around 1500 s^{-1} (Figure 4A). However, when thrombus grew to a larger size, the arteriolar lumen was narrowed, which resulted in increase in shear rates.[23] Then, the distal C-terminal truncation of

ADAMTS13 significantly reduced the occlusion time compared with full-length ADAMTS13 (Figure 4B). Therefore, the distal C-terminal domains are important for ADAMTS13 to sufficiently down-regulate thrombogenesis under high shear rate in vivo as well as in vitro. After the induction of systemic platelet aggregation by challenge with a mixture of collagen and epinephrine, consumptive thrombocytopenia was also enhanced by the distal C-terminal truncation of ADAMTS13 in 129/Sv mice (Figure 5), supporting the idea that the distal C-terminal domains are required for optimal down-regulation of platelet aggregation in vivo. The complete deficiency of ADAMTS13 in 129/Sv significantly accelerated thrombus growth to injured vessel wall and systemic thrombi compared with 129/Sv mice with truncation of the distal C-terminal domains in ADAMTS13 (Figures 4,5). Therefore, we can conclude that the distal C-terminally truncated ADAMTS13 has significantly decreased activity in limiting thrombosis in vivo.

The binding of platelets to VWF is reported to accelerate the cleavage of VWF by ADAMTS13 under static[35] and flow[36] conditions in vitro. It has also been shown that ADAMTS13 can cleave platelet-bound VWF multimers[37] and limit thrombus formation through the cleavage of VWF at the surface of forming thrombi[28] in in vitro flow chamber systems. Therefore, in our experimental settings, ADAMTS13 attenuates thrombus growth, possibly through the cleavage of VWF multimers bound on the surface of platelet-rich thrombi under high shear rate. The distal C-terminal domains may be necessary for ADAMTS13 to efficiently recognize and cleave platelet-bound VWF multimers on a growing thrombus. Conceivably, the distal C-terminal domains may contribute to the interaction with unidentified ADAMTS13-binding cofactors localized on the surface of platelets or subendothelium, and this interaction may be necessary for ADAMTS13 to control VWF-mediated thrombus formation. However, we cannot rule out the possibility that the distal C-terminal domains of ADAMTS13 contribute to the prevention of thrombosis independent from the VWF-cleaving activity of ADAMTS13, nevertheless VWF has been suggested as the only relevant substrate for ADAMTS13[38] and functions of ADAMTS13 other than its VWF-cleaving activity have yet to be reported.

The distal C-terminally truncated ADAMTS13 is expressed in a lot of mouse strains including the BALB/c, C3H/He, C57BL/6, and DBA/2 strains as substitute for the full-length form.[14,15] Our present results suggest that thrombotic response in these strains would be increased, at least partially, by their incomplete ADAMTS13 activity. This should be taken into account when studying genetically modified mice with heterogeneous genetic background.

In summary, our results define the role of the distal C-terminal domains in ADAMTS13 in vivo. Deletion of the C-terminal 2 Tsp1 and 2 CUB domains permits normal size distribution of plasma VWF multimers under steady state, but exacerbates platelet thrombosis after thrombogenic stimulation in mice. Thus, the distal C-terminally truncated ADAMTS13 is not fully active in vivo. These distal C-terminal domains of ADAMTS13 may play a role in the efficient processing of VWF multimers during platelet thrombus growth, and thus their functions may become increasingly important when vascular damage is induced.

Authorship

Contribution: F.B. designed research, performed experiments, analyzed data, and wrote the paper; A.K.C. performed experiments, contributed vital analytical tools, and analyzed the data; K.K. designed research, performed experiments, and wrote the paper; J.Y. performed experiments and analyzed data; S.M. and D.D.W. contributed vital analytical tools and interpreted the data; and T.M. designed research and wrote the paper.

Conflict-of-interest disclosure: The authors declare no competing financial interests.

Correspondence: Toshiyuki Miyata, National Cardiovascular Center Research Institute, 5-7-1 Fujishirodai, Suita, Osaka 565-8565, Japan; e-mail: miyata@ri.ncvc.go.jp.

References

1. Dong JF. Structural and functional correlation of ADAMTS13. Curr Opin Hematol. 2007;14:270-276.

2. Bergmeier W, Chauhan AK, Wagner DD. Glycoprotein Ibalpha and von Willebrand factor in primary platelet adhesion and thrombus formation: lessons from mutant mice. Thromb Haemost. 2008;99:264-270.

3. Tsai HM. Thrombotic thrombocytopenic purpura: a thrombotic disorder caused by ADAMTS13 deficiency. Hematol Oncol Clin North Am. 2007;21:609-632.

4. Zheng XL, Sadler JE. Pathogenesis of thrombotic microangiopathies. Annu Rev Pathol. 2008;3:249-277.

5. Desch KC, Motto DG. Thrombotic thrombocytopenic purpura in humans and mice. Arterioscler Thromb Vasc Biol. 2007;27:1901-1908.

6. Soejima K, Matsumoto M, Kokame K, et al. ADAMTS-13 cysteine-rich/spacer domains are functionally essential for von Willebrand factor cleavage. Blood. 2003;102:3232-3237.

7. Zheng X, Nishio K, Majerus EM, Sadler JE. Cleavage of von Willebrand factor requires the spacer domain of the metalloprotease ADAMTS13. J Biol Chem. 2003;278:30136-30141.

8. Ai J, Smith P, Wang S, Zhang P, Zheng XL. The proximal carboxyl-terminal domains of ADAMTS13 determine substrate specificity and are all required for cleavage of von Willebrand factor. J Biol Chem. 2005;280:29428-29434.

9. Majerus EM, Anderson PJ, Sadler JE. Binding of ADAMTS13 to von Willebrand factor. J Biol Chem. 2005;280:21773-21778.

10. Tao Z, Wang Y, Choi H, et al. Cleavage of ultra-large multimers of von Willebrand factor by C-terminal-truncated mutants of ADAMTS-13 under flow. Blood. 2005;106:141-143.

11. Tao Z, Peng Y, Nolasco L, et al. Recombinant CUB-1 domain polypeptide inhibits the cleavage of ULVWF strings by ADAMTS13 under flow conditions. Blood. 2005;106:4139-4145.

12. Gao W, Anderson PJ, Majerus EM, Tuley EA, Sadler JE. Exosite interactions contribute to tension-induced cleavage of von Willebrand factor by the antithrombotic ADAMTS13 metalloprotease. Proc Natl Acad Sci U S A. 2006;103:19099-19104.

13. Zhang P, Pan W, Rux AH, Sachais BS, Zheng XL. The cooperative activity between the carboxyl-terminal TSP1 repeats and the CUB domains of ADAMTS13 is crucial for recognition of von Willebrand factor under flow. Blood. 2007;110:1887-1894.

14. Banno F, Kaminaka K, Soejima K, Kokame K, Miyata T. Identification of strain-specific variants of mouse Adamts13 gene encoding von Willebrand factor-cleaving protease. J Biol Chem. 2004;279:30896-30903.

15. Zhou W, Bouhassira EE, Tsai HM. An IAP retrotransposon in the mouse ADAMTS13 gene creates ADAMTS13 variant proteins that are less effective in cleaving von Willebrand factor multimers. Blood. 2007;110:886-893.

16. Banno F, Miyata T. Biology of an antithrombotic factor-ADAMTS13. In: Tanaka K, Davie EW, eds. Recent Advances in Thrombosis and Hemostasis. Berlin, Germany: Springer; 2008:162-176.

17. Banno F, Kokame K, Okuda T, et al. Complete deficiency in ADAMTS13 is prothrombotic, but it alone is not sufficient to cause thrombotic thrombocytopenic purpura. Blood. 2006;107:3161-3166.

18. Miyata T, Kokame K, Banno F, Shin Y, Akiyama M. ADAMTS13 assays and ADAMTS13-deficient mice. Curr Opin Hematol. 2007;14:277-283.

19. Kokame K, Matsumoto M, Fujimura Y, Miyata T. VWF73, a region from D1596 to R1668 of von Willebrand factor, provides a minimal substrate for ADAMTS-13. Blood. 2004;103:607-612.

20. Kokame K, Nobe Y, Kokubo Y, Okayama A, Miyata T. FRETS-VWF73, a first fluorogenic substrate for ADAMTS13 assay. Br J Haematol. 2005;129:93-100.

21. Tsuji S, Sugimoto M, Miyata S, Kuwahara M, Kinoshita S, Yoshioka A. Real-time analysis of mural thrombus formation in various platelet aggregation disorders: distinct shear-dependent roles of platelet receptors and adhesive proteins under flow. Blood. 1999;94:968-975.

22. Chauhan AK, Motto DG, Lamb CB, et al. Systemic antithrombotic effects of ADAMTS13. J Exp Med. 2006;203:767-776.

23. Ni H, Denis CV, Subbarao S, et al. Persistence of platelet thrombus formation in arterioles of mice lacking both von Willebrand factor and fibrinogen. J Clin Invest. 2000;106:385-392.

24. Frenette PS, Moyna C, Hartwell DW, Lowe JB, Hynes RO, Wagner DD. Platelet-endothelial interactions in inflamed mesenteric venules. Blood. 1998;91:1318-1324.

25. DiMinno G, Silver MJ. Mouse antithrombotic assay: a simple method for the evaluation of antithrombotic agents in vivo. Potentiation of antithrombotic activity by ethyl alcohol. J Pharmacol Exp Ther. 1983;225:57-60.

26. Jackson SP. The growing complexity of platelet aggregation. Blood. 2007;109:5087-5095.

27. Konstantinides S, Ware J, Marchese P, Almus-Jacobs F, Loskutoff DJ, Ruggeri ZM. Distinct antithrombotic consequences of platelet glycoprotein Ibalpha and VI deficiency in a mouse model of arterial thrombosis. J Thromb Haemost. 2006;4:2014-2021.

28. Shida Y, Nishio K, Sugimoto M, et al. Functional imaging of shear-dependent activity of ADAMTS13 in regulating mural thrombus growth under whole blood flow conditions. Blood. 2008;111:1295-1298.

29. Smyth SS, Reis ED, Vaananen H, Zhang W, Coller BS. Variable protection of beta 3-integrin–deficient mice from thrombosis initiated by different mechanisms. Blood. 2001;98:1055-1062.

30. Cui J, Eitzman DT, Westrick RJ, et al. Spontaneous thrombosis in mice carrying the factor V Leiden mutation. Blood. 2000;96:4222-4226.

31. Weiler H, Lindner V, Kerlin B, et al. Characterization of a mouse model for thrombomodulin deficiency. Arterioscler Thromb Vasc Biol. 2001;21:1531-1537.

32. Suh TT, Holmback K, Jensen NJ, et al. Resolution of spontaneous bleeding events but failure of pregnancy in fibrinogen-deficient mice. Genes Dev. 1995;9:2020-2033.

33. Toomey JR, Kratzer KE, Lasky NM, Broze GJ Jr. Effect of tissue factor deficiency on mouse and tumor development. Proc Natl Acad Sci U S A. 1997;94:6922-6926.

34. Motto DG, Chauhan AK, Zhu G, et al. Shigatoxin triggers thrombotic thrombocytopenic purpura in genetically susceptible ADAMTS13-deficient mice. J Clin Invest. 2005;115:2752-2761.

35. Nishio K, Anderson PJ, Zheng XL, Sadler JE. Binding of platelet glycoprotein Ibalpha to von Willebrand factor domain A1 stimulates the cleavage of the adjacent domain A2 by ADAMTS13. Proc Natl Acad Sci U S A. 2004;101:10578-10583.

36. Shim K, Anderson PJ, Tuley EA, Wiswall E, Sadler JE. Platelet-VWF complexes are preferred substrates of ADAMTS13 under fluid shear stress. Blood. 2008;111:651-657.

37. Donadelli R, Orje JN, Capoferri C, Remuzzi G, Ruggeri ZM. Size regulation of von Willebrand factor-mediated platelet thrombi by ADAMTS13 in flowing blood. Blood. 2006;107:1943-1950.

38. Chauhan AK, Walsh MT, Zhu G, Ginsburg D, Wagner DD, Motto DG. The combined roles of ADAMTS13 and VWF in murine models of TTP, endotoxemia, and thrombosis. Blood. 2008;111:3452-3457.

Production, crystallization and preliminary crystallographic analysis of an exosite-containing fragment of human von Willebrand factor-cleaving proteinase ADAMTS13

Masashi Akiyama,[a] Soichi Takeda,[a] Koichi Kokame,[a] Junichi Takagi[b] and Toshiyuki Miyata[a]*

[a]National Cardiovascular Center Research Institute, 5-7-1 Fujishirodai, Suita, Osaka 565-8565, Japan, and [b]Laboratory of Protein Synthesis and Expression, Institute for Protein Research, Osaka University, 3-2 Yamadaoka, Suita, Osaka 565-0871, Japan

Correspondence e-mail: miyata@ri.ncvc.go.jp

ADAMTS13 is a reprolysin-type metalloproteinase belonging to the ADAMTS (a disintegrin and metalloproteinase with thrombospondin type 1 motif) family. It specifically cleaves plasma von Willebrand factor (VWF) and regulates platelet adhesion and aggregation. ADAMTS13 is a multi-domain enzyme. In addition to the N-terminal metalloproteinase domain, the ancillary domains, including a disintegrin-like domain, a thrombospondin-1 type 1 repeat, a Cys-rich domain and a spacer domain, are required for VWF recognition and cleavage. In the present study, a fragment of the ADAMTS13 ancillary domains (ADAMTS13-DTCS; residues 287–685) was expressed using CHO Lec cells, purified and crystallized. Diffraction data sets were collected using the SPring-8 beamline. Two ADAMTS13-DTCS crystals with distinct unit-cell parameters generated data sets to 2.6 and 2.8 Å resolution, respectively.

1. Introduction

von Willebrand factor (VWF) is a plasma glycoprotein that is involved in platelet-dependent haemostasis (Sadler, 1998). VWF is primarily synthesized in vascular endothelial cells and megakaryocytes and is released into the plasma as ultralarge multimeric forms (UL-VWF) that are highly active in platelet adhesion and aggregation. A plasma metalloproteinase, ADAMTS13, specifically cleaves the Tyr1605-Met1606 peptidyl bond within the A2 domain of VWF (Dent *et al.*, 1990). Cleavage of UL-VWF into smaller forms by ADAMTS13 limits platelet thrombus formation. A deficiency of ADAMTS13 enzymatic activity caused by either genetic mutations in the ADAMTS13 gene or acquired autoantibodies against ADAMTS13 results in the accumulation of UL-VWF in plasma. This leads to the formation of disseminated platelet-rich microthrombi in arterioles, which is one of the characteristic pathogenic features of thrombotic thrombocytopaenic purpura (TTP), a life-threatening systemic disease (Tsai, 2009). Conversely, excessive cleavage of VWF causes von Willebrand disease type 2A (Sadler, 2005).

Human ADAMTS13 consists of 1427 amino acids and has a modular structure comprising a signal peptide, a short propeptide, a metalloproteinase domain (M), a disintegrin-like domain (D), a thrombospondin-1 type 1 repeat (T1), a Cys-rich domain (C), a spacer domain (S), seven additional type 1 repeats (T2–T8) and two CUB (C1r/C1s, urinary epidermal growth factor, bone morphogenic protein) domains (Levy *et al.*, 2001; Soejima *et al.*, 2001; Zheng *et al.*, 2001). C-terminal truncation of ADAMTS13 after the C but not the S domain results in severe loss of proteolytic activity towards VWF (Soejima *et al.*, 2003; Zheng *et al.*, 2003). Therefore, in addition to the M domain, the ancillary domains including the D, T, C and S domains (DTCS) are necessary for normal ADAMTS13 activity, although the distal C-terminal domains are required for regulation of *in vivo* thrombus formation under high-shear conditions (Banno et al., 2009). We have previously reported a minimal functional substrate consisting of 73 amino-acid residues of the C-terminal region of the VWF A2 domain (Asp1596–Arg1668) and designated VWF73 (Kokame *et al.*, 2004; Miyata *et al.*, 2007). A recent study has shown that the VWF-binding exosites located in the T, C and S domains interact with different segments of VWF73 (Gao *et al.*, 2008). These interactions increased the VWF-binding affinity and rate of substrate cleavage by
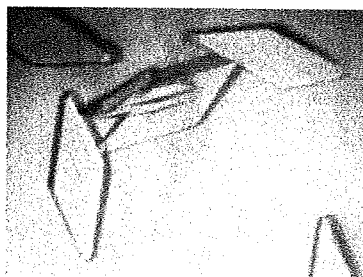
300-fold. At least 16 causative missense mutations for congenital TTP and five missense polymorphisms in the ADAMTS13 gene have been identified within the DTCS region (Levy *et al.*, 2001; Kokame *et al.*, 2002; Banno & Miyata, 2008). Although most TTP-causative mutant proteins are likely to show secretion deficiency, a P475S polymorphism variant showed normal secretion but reduced VWF-cleaving activity (Kokame *et al.*, 2002; Akiyama *et al.*, 2008). Detailed structural information on exosite-containing domains will help in understanding the structure-based mechanism of substrate recognition and specificity and the effects of TTP-causative mutations and common polymorphisms. To date, crystal structures of the M and D domains of three human ADAMTS-family proteins, ADAMTS1, ADAMTS4 and ADAMTS5, have been reported (Gerhardt *et al.*, 2007; Mosyak *et al.*, 2008; Shieh *et al.*, 2008). However, no crystal structures of exosite-containing fragments of ADAMTSs have been reported.

Here, we report the expression and purification of the exosite-containing human ADAMTS13-DTCS fragment using mammalian CHO Lec cells with mutations in multiple glycosylation-related genes. Proteins obtained from this cell line are suitable for crystallization because their restricted and homogeneous glycosylation improves the packing of the protein molecules. We also report the results of our crystallization and preliminary X-ray studies of ADAMTS13-DTCS.

2. Methods

2.1. Expression and purification of ADAMTS13-DTCS

An ADAMTS13 cDNA (AB069698) fragment corresponding to amino-acid residues 287–685 (ADAMTS13-DTCS) was amplified by PCR and cloned into a mammalian expression vector based on pcDNA3.1/Myc-His (Invitrogen), which has a mouse *Nid1* signal sequence (Yasui *et al.*, 2007). The nucleotide sequence was confirmed by dye-terminator sequencing. The ADAMTS13-DTCS fragment expressed from this vector contains a tobacco etch virus (TEV) proteinase cleavage site (Glu-Asn-Leu-Tyr-Phe-Gln/Gly) followed by tandem His-tag sequences at the C-terminus. We transfected the plasmid into CHO Lec 3.2.8.1 cells (Stanley, 1989) by electroporation and selected colonies resistant to G418 (3 mg ml^{-1}) on 96-well plates in α-minimal essential medium supplemented with 5% foetal bovine serum for 10 d. ADAMTS13-DTCS levels in the media of 48 G418-resistant colonies were examined by Western blotting with anti-6×His antibody (Sigma–Aldrich, St Louis, Missouri, USA). The clone with the highest secretion level of ADAMTS13-DTCS was cultured in the medium containing 0.5 mg ml^{-1} G418 by the roller-bottle method and the medium was collected every 3 d. The ADAMTS13-DTCS was recovered from the culture medium by 50%(*w/v*) ammonium sulfate precipitation and was purified by Ni–NTA agarose chromatography (Sigma–Aldrich). The eluted ADAMTS13-DTCS was incubated with TEV proteinase for 12 h at 297 K to remove the C-terminal tags. After dialysis in a buffer consisting of 10 m*M* MES and 100 m*M* NaCl pH 6.0, the digest was applied onto a Hi-Trap SP HP cation-exchange column (GE Healthcare, Buckinghamshire, England). The column was washed with the same buffer and ADAMTS13-DTCS was eluted with a linear gradient of NaCl (0.1–0.7 *M*) in 10 m*M* MES pH 6.0. Fractions were analyzed by SDS–PAGE under reducing conditions (Fig. 1). The fractions rich in ADAMTS13-DTCS (lanes 5 and 6) were combined, dialyzed against 10 m*M* MES pH 6.0 and concentrated using a Vivaspin-5 separation device (30 kDa molecular-weight cutoff;

Sartorius, Edgewood, New York, USA) to a final concentration of ~10 mg ml^{-1} for crystallization.

2.2. Crystallization screening

Initial screening for crystallization conditions for ADAMTS-DTCS was carried out by the sitting-drop vapour-diffusion method using Index Screen, SaltRx Screen, PEG/Ion Screen, Grid Screen MPD and Grid Screen Ammonium Sulfate kits (Hampton Research, Aliso Viejo, California, USA). A volume of 0.1 μl protein solution was manually mixed with an equal amount of reservoir solution and the droplets were allowed to equilibrate against 0.1 ml reservoir solution at 293 K for 24 h.

2.3. Diffraction data collection

For X-ray measurements, crystals were soaked in a solution containing 20% glycerol, 26% PEG 1500, 100 m*M* MES pH 6.0 for cryoprotection prior to flash-freezing and were immediately exposed to a stream of nitrogen gas at 100 K. Preliminary X-ray data were collected using an in-house X-ray diffractometer (Micromax-007 X-ray generator with an R-AXIS VII imaging-plate detector; Rigaku, Tokyo, Japan) and diffraction-quality crystals were selected for data acquisition using the SPring-8 beamline. All the diffraction data sets were collected on beamline BL41XU at 100 K using an ADSC Quantum 310R detector and the diffraction images were processed using *HKL*-2000 software (Minor *et al.*, 2006).

3. Results and discussion

3.1. Protein preparation

We first attempted to express ADAMTS13-DTCS in *Escherichia coli* and insect cells. The expressed ADAMTS13-DTCS formed inclusion bodies and renaturation of ADAMTS13-DTCS did not succeed. We then tried to express ADAMTS13-DTCS in mammalian cells. As ADAMTS13-DTCS contains four potential N-glycosylation sites, we used the CHO Lec 3.2.8.1 cell line for stable expression. This cell line has four different mutated genes that are involved in the N- and O-glycosylation pathways (Stanley, 1989). Preliminary experiments showed that the endogenous signal and propeptide sequences of ADAMTS13 resulted in low protein secretion. We replaced the
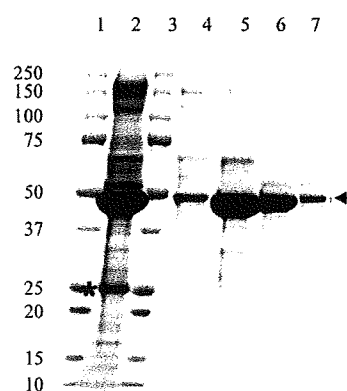

Figure 1
SDS–PAGE analysis of ADAMTS13-DTCS fractions from Hi-Trap SP HP cation chromatography. Proteins were analyzed by SDS–PAGE and stained with Coomassie Brilliant Blue. Lanes 1 and 3, molecular-weight markers (kDa); lane 2, pooled Ni–NTA eluate treated with TEV proteinase; lanes 4–7, eluate fractions Nos. 5–8, respectively, from the Hi-Trap SP HP column. Arrow, ADAMTS13-DTCS. Asterisk, TEV proteinase.

signal sequence and prosequence with the mouse *Nid1* signal sequence (Mann *et al.*, 1989). This replacement dramatically increased the secretion of ADAMTS13-DTCS into the medium. ADAMTS13-DTCS was purified by Ni–NTA chromatography followed by Hi-Trap SP cation-exchange chromatography. The molecular weight of the recombinant protein, 45 kDa, estimated by SDS–PAGE coincided well with the estimated molecular weight of 46 kDa (Fig. 1). Fractions (Fig. 1, lanes 5 and 6) from the Hi-Trap SP column were combined and used for crystallization without further purification. Approximately 6 mg ADAMTS13-DTCS was recovered from 20 l culture medium.

3.2. Crystallization

Of the 288 initial crystallization conditions tested, 20 yielded microcrystals (Fig. 2*a*). Using solution No. 4 of the PEG/Ion Screen kit [0.2 *M* lithium chloride, 20%(*w/v*) PEG 3350 pH 6.8] as a starting condition, the pH of the mother liquor, the concentration and molecular weight of the PEG and the species and concentrations of salts and additives were optimized. The combination of refinement of the crystallization conditions and an increase in the protein concentration (to ~20 mg ml^{-1}) improved the size of the crystals. Single crystals were obtained from drops made up of 0.5 µl protein solution and 0.5 µl reservoir solution [26%(*w/v*) PEG 1500, 100 m*M* MES pH 6.0] supplemented with a one-fifth volume of 40%(*w/w*) pentaerythritol ethoxylate (3/4 EO/OH; Additive Screen solution No. 52; Hampton Research). Crystals with dimensions of 300 × 100 × 50 µm were formed after 3–7 d at 293 K (Fig. 2*b*).
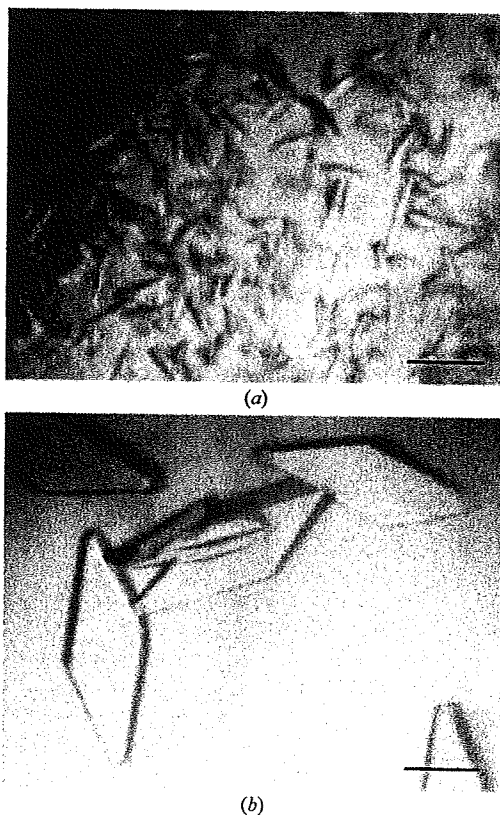

(*a*)

(*b*)

Figure 2
Crystals of human ADAMTS13-DTCS grown by the sitting-drop method. (*a*) Microcrystals obtained from solution No. 4 of the PEG/Ion Screen kit. (*b*) Crystals obtained using the optimized conditions. The scale bars indicate 0.1 mm.

Table 1
Data-collection statistics for ADAMTS13-DTCS crystals.

Values in parentheses are for the highest resolution shell. A single crystal was used for measurement for each data set.

	Form 1	Form 2
Space group	*C*2	*C*2
Unit-cell parameters		
a (Å)	152.7	138.6
b (Å)	52.9	51.4
c (Å)	76.2	76.4
β (°)	111.4	106.7
Wavelength (Å)	1.0	1.0
Resolution (Å)	50–2.60 (2.69–2.60)	30–2.80 (2.90–2.80)
No. of unique reflections	16867 (1272)	12811 (1259)
R_{merge}†	0.052 (0.176)	0.062 (0.403)
$I/\sigma(I)$	19.3 (5.7)	13.3 (3.5)
Completeness (%)	95.3 (72.7)	99.5 (99.3)
Redundancy	3.5 (2.9)	3.7 (3.6)
Matthews value (Å^3 Da^{-1})	2.64	2.39
Solvent content (%)	53.4	48.6

† $R_{merge} = \sum_{hkl} \sum_{i} |I_i(hkl) - \langle I(hkl)\rangle| / \sum_{hkl} \sum_{i} I_i(hkl)$, where $I_i(hkl)$ is the *i*th intensity measurement of reflection *hkl* and $\langle I(hkl)\rangle$ is its weighted average.

3.3. X-ray analysis

All diffraction data sets were acquired using the oscillation method on beamline BL41XU at a wavelength of 1.0 Å. The oscillation angle was 1.0° for all data sets. The native data sets for form 1 and form 2 contained 16 867 (2.60 Å resolution) and 12 811 (2.80 Å resolution) unique reflections, respectively. The asymmetric unit was estimated to contain one molecule, with corresponding crystal volume per protein weights of 2.7 and 3.1 Å^3 Da^{-1} for crystal forms 1 and 2, respectively. Solvent-content estimations based on a single copy of the molecule per asymmetric unit gave values of 53.4% and 48.6% for crystal forms 1 and 2, respectively. The X-ray data showed that the two crystal forms have different unit-cell parameters even when they are obtained under identical conditions. The variation in crystal packing might reflect the mobility of the domains in ADAMTS13-DTCS. The statistics of the data sets are summarized in Table 1.

3.4. Screening of heavy-atom derivatives

We attempted experimental phasing using heavy-atom derivatives because molecular replacement was not an option owing to the lack of related structures. The limited availability of single large crystals owing to the small amount of ADAMTS13-DTCS and its tendency to form multiple crystals produced difficulties in the search for heavy-atom derivatives. Therefore, we focused on investigating the colouring of crystals on heavy-atom soaking, which can be a good indication of heavy-atom binding. We selected 13 coloured compounds (Au-6, M1-10, M-11, M1-14, M1-15, M1-16, M1-17, M2-2, M2-3, M2-5, M2-16, M2-17 and M2-18) from Heavy Atom Screens (Hampton Research) and soaked small crystals in reservoir solution supplemented with each of these compounds. After several hours, we found that three osmium-containing compounds, ammonium hexabromoosmate (M2-16), potassium hexachloroosmate (M2-17) and osmium chloride (M2-18), were heavily absorbed into the crystals. To examine the X-ray diffraction from these potential derivatives, we prepared larger single crystals. We checked these using the in-house X-ray facility and well diffracting crystals were shipped for data acquisition at SPring-8. Structural analysis is now in progress using data obtained from the derivative soaked in the osmium chloride solution.

crystallization communications

References

Akiyama, M., Kokame, K. & Miyata, T. (2008). *J. Thromb. Haemost.* **6**, 1830–1832.

Banno, F., Chauhan, A. K., Kokame, K., Yang, J., Miyata, S., Wagner, D. D. & Miyata, T. (2009). *Blood*, **113**, 5323–5329.

Banno, F. & Miyata, T. (2008). *Recent Advances in Thrombosis and Hemostasis*, edited by K. Tanaka & E. W. Davie, pp. 162–176. Tokyo: Springer.

Dent, J. A., Berkowitz, S. D., Ware, J., Kasper, C. K. & Ruggeri, Z. M. (1990). *Proc. Natl Acad. Sci. USA*, **87**, 6306–6310.

Gao, W., Anderson, P. J. & Sadler, J. E. (2008). *Blood*, **112**, 1713–1719.

Gerhardt, S., Hassall, G., Hawtin, P., McCall, E., Flavell, L., Minshull, C., Hargreaves, D., Ting, A., Pauptit, R. A., Parker, A. E. & Abbott, W. M. (2007). *J. Mol. Biol.* **373**, 891–902.

Kokame, K., Matsumoto, M., Fujimura, Y. & Miyata, T. (2004). *Blood*, **103**, 607–612.

Kokame, K., Matsumoto, M., Soejima, K., Yagi, H., Ishizashi, H., Funato, M., Tamai, H., Konno, M., Kamide, K., Kawano, Y., Miyata, T. & Fujimura, Y. (2002). *Proc. Natl Acad. Sci. USA*, **99**, 11902–11907.

Levy, G. G. *et al.* (2001). *Nature (London)*, **413**, 488–494.

Mann, K., Deutzmann, R., Aumailley, M., Timpl, R., Raimondi, L., Yamada, Y., Pan, T. C., Conway, D. & Chu, M. L. (1989). *EMBO J.* **8**, 65–72.

Minor, W., Cymborowski, M., Otwinowski, Z. & Chruszcz, M. (2006). *Acta Cryst.* D**62**, 859–866.

Miyata, T., Kokame, K., Banno, F., Shin, Y. & Akiyama, M. (2007). *Curr. Opin. Hematol.* **14**, 277–283.

Mosyak, L. *et al.* (2008). *Protein Sci.* **17**, 16–21.

Sadler, J. E. (1998). *Annu. Rev. Biochem.* **67**, 395–424.

Sadler, J. E. (2005). *Annu. Rev. Med.* **56**, 173–191.

Shieh, H. S., Mathis, K. J., Williams, J. M., Hills, R. L., Wiese, J. F., Benson, T. E., Kiefer, J. R., Marino, M. H., Carroll, J. N., Leone, J. W., Malfait, A. M., Arner, E. C., Tortorella, M. D. & Tomaselli, A. (2008). *J. Biol. Chem.* **283**, 1501–1507.

Soejima, K., Matsumoto, M., Kokame, K., Yagi, H., Ishizashi, H., Maeda, H., Nozaki, C., Miyata, T., Fujimura, Y. & Nakagaki, T. (2003). *Blood*, **102**, 3232–3237.

Soejima, K., Mimura, N., Hirashima, M., Maeda, H., Hamamoto, T., Nakagaki, T. & Nozaki, C. (2001). *J. Biochem.* **130**, 475–480.

Stanley, P. (1989). *Mol. Cell. Biol.* **9**, 377–383.

Tsai, H. M. (2009). *Kidney Int. Suppl.*, pp. S11–S14.

Yasui, N., Nogi, T., Kitao, T., Nakano, Y., Hattori, M. & Takagi, J. (2007). *Proc. Natl Acad. Sci. USA*, **104**, 9988–9993.

Zheng, X., Chung, D., Takayama, T. K., Majerus, E. M., Sadler, J. E. & Fujikawa, K. (2001). *J. Biol. Chem.* **276**, 41059–41063.

Zheng, X., Nishio, K., Majerus, E. M. & Sadler, J. E. (2003). *J. Biol. Chem.* **278**, 30136–30141.

Crystal structures of the noncatalytic domains of ADAMTS13 reveal multiple discontinuous exosites for von Willebrand factor

Masashi Akiyama[a,1], Soichi Takeda[a,1,2], Koichi Kokame[a], Junichi Takagi[b], and Toshiyuki Miyata[a,2]

[a]National Cardiovascular Center Research Institute, Suita, Osaka 565-8565, Japan; and [b]Laboratory of Protein Synthesis and Expression, Institute for Protein Research, Osaka University, Suita, Osaka 565-0871, Japan

ADAMTS13 specifically cleaves plasma von Willebrand factor (VWF) and thereby controls VWF-mediated platelet thrombus formation. Severe deficiencies in ADAMTS13 can cause life-threatening thrombotic thrombocytopenic purpura. Here, we determined 2 crystal structures of ADAMTS13-DTCS (residues 287–685), an exosite-containing human ADAMTS13 fragment, at 2.6-Å and 2.8-Å resolution. The structures revealed folding similarities between the disintegrin-like (D) domain and the N-terminal portion of the cysteine-rich domain (designated the C_A domain). The spacer (S) domain forms a globular functional unit with a 10-stranded β-sandwich fold that has multiple interaction sites with the C_A domain. We expressed 25 structure-based mutants of ADAMTS13-MDTCS (residues 75–685) and measured their enzymatic activity. We identified 3 VWF-binding exosites on the linearly aligned discontinuous surfaces of the D, C_A, and S domains traversing the W-shaped molecule. Since the MDTCS domains are conserved among ADAMTS family proteins, the structural framework of the multiple enzyme-substrate interactions identified in the ADAMTS13-VWF system provides the basis for a common substrate recognition mode in this class of proteinases.

hemostasis | metalloproteinase | modular protein | substrate recognition

T he human ADAMTS (a disintegrin-like and metalloproteinase with thrombospondin type-1 motif) family is composed of 19 genes that encode extracellular multidomain enzymes containing a reprolysin-type metalloproteinase domain and several conserved domains following the metalloproteinase domain (1). In contrast to the phylogenetically related ADAM (a disintegrin and metalloproteinase) family proteins, most of which have a transmembrane and a cytoplasmic domain in the C-terminal region (2), ADAMTSs are secretory proteinases that lack these domains and instead have at least 1 thrombospondin-1 (TSP-1) type-1 repeat (TSR). ADAMTSs have diverse functions including procollagen processing, aggrecan degradation, and organogenesis (1). ADAMTS13 controls platelet thrombus formation through cleavage of the von Willebrand factor (VWF).

VWF is a plasma glycoprotein that plays an essential role in platelet-dependent hemostasis (3, 4). VWF mediates platelet adherence to damaged blood vessels through interactions with glycoprotein Ib on the platelet surface and collagen in the subendothelium and contributes to platelet aggregation through interactions with integrin $\alpha_{IIb}\beta_3$. VWF, synthesized mainly in vascular endothelial cells, contains 2,050 aa residues and is released into the plasma as disulfide-bonded ultralarge VWF (UL-VWF) multimers having a mass greater than 20,000 kDa. In healthy individuals, UL-VWF multimers undergo limited proteolytic processing (5). ADAMTS13 specifically cleaves the Tyr-1605-Met-1606 peptidyl bond within the A2 domain of VWF (6) in a fluid shear-stress-dependent manner (7). Because VWF multimers have an alternate head-to-head and tail-to-tail disulfide-bonded architecture between neighboring subunits, cleavage by ADAMTS13 gives rise to a series of circulating multimers with molecular masses ranging from 500 to 15,000 kDa. Control of the size

distribution of VWF multimers is important for normal hemostasis, as large multimers are hemostatically more active than small multimers (3). Deficiencies in ADAMTS13 activity, caused either by genetic mutations in the ADAMTS13 gene or by acquired inhibitory autoantibodies directed against the ADAMTS13 protein, results in the accumulation of UL-VWF in the plasma (8–11). The UL-VWF accumulation leads to the formation of disseminated platelet-rich microthrombi in the microvasculature, which results in the life-threatening disease, thrombotic thrombocytopenic purpura (TTP).

The human ADAMTS13 gene encodes a precursor protein of 1,427 aa with a modular structure consisting of a signal peptide, a propeptide (P), a metalloproteinase (M) domain, a disintegrin-like (D) domain, a TSR (T1), a cysteine-rich (C) region, a spacer (S), 7 TSRs (T2–T8), and 2 CUB (complement components C1rC1s/ urinary epidermal growth factor/bone morphogenetic protein-1) domains (11–13). The M domain of ADAMTS13 alone is not sufficient for recognition and specific cleavage of VWF, but full VWF-cleaving activity is achieved in vitro with an M-D-T1-C-S domain fragment (14–17). In addition, antibodies isolated from idiopathic TTP patients commonly inhibit ADAMTS13 activity by binding to the C and S domains of ADAMTS13 (14, 18, 19). Collectively, these observations indicate that the noncatalytic domains, especially the proximal C-terminal domains including the D, T1, C, and S domains (designated ADAMTS13-DTCS), are essential for recognition of VWF. The crystal structures of the MD domains (ADAMTS-MDs) of ADAMTS1 (20), ADAMTS4 (21), and ADAMTS5 (21) have been determined, but no structural information is currently available for the T1, C, and S domains of ADAMTS proteins. To gain insight into the molecular mechanism of VWF recognition by ADAMTS13, we solved the crystal structures of ADAMTS13-DTCS (residues 287–685) and performed a series of structure-based mutagenesis experiments to identify VWF-binding exosites. The present structure is the first for the TCS domains of any ADAMTS family member and will provide a template for understanding the role of these domains in substrate recognition by ADAMTS proteins.

Results

Structure Determination. The structure of ADAMTS13-DTCS was solved using the multiple-wavelength anomalous dispersion
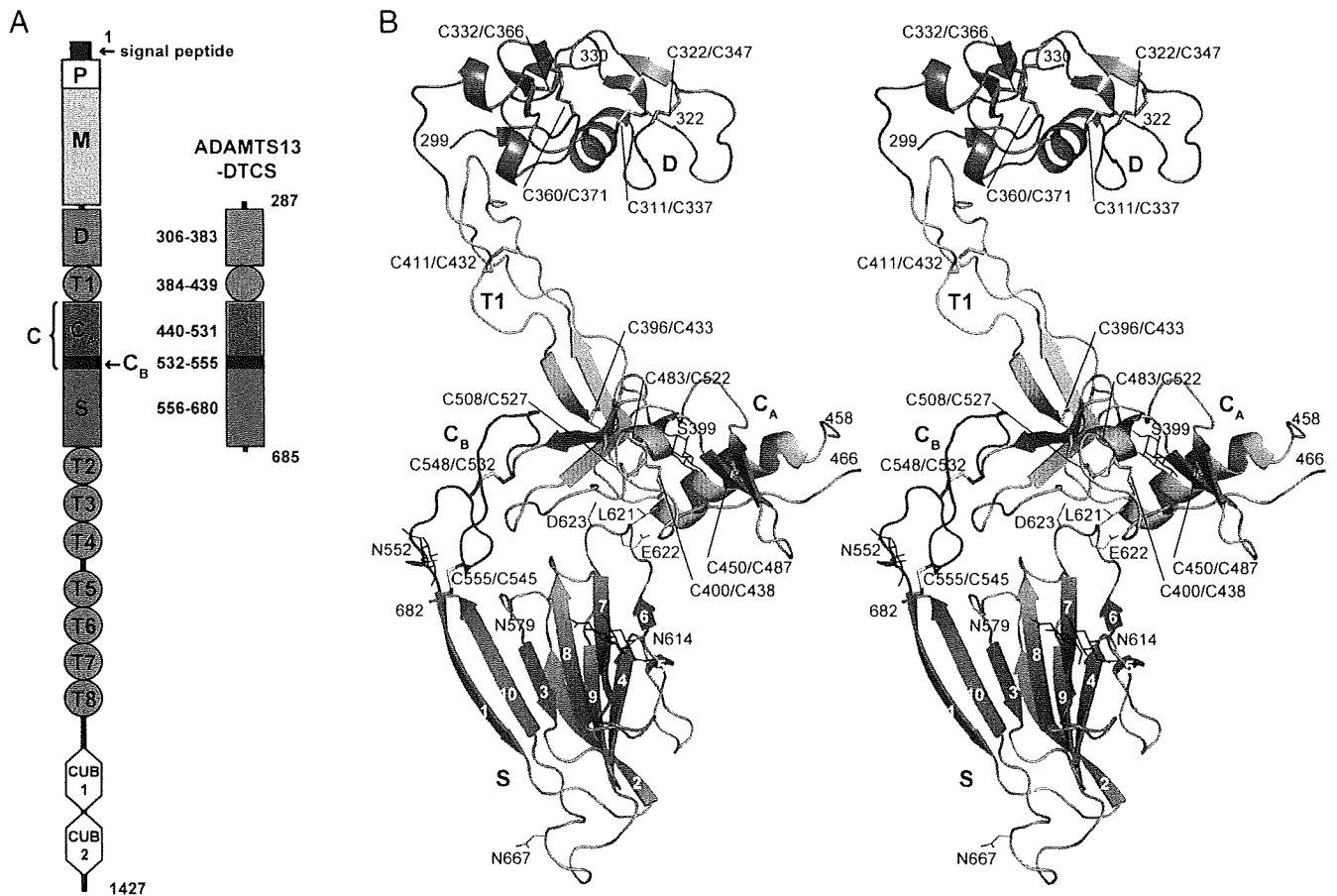
Fig. 1. Structure of ADAMTS13-DTCS. (*A*) Schematic representation of the domain structures of full-length ADAMTS13 and ADAMTS13-DTCS. (*B*) Ribbon structure of ADAMTS13-DTCS (form-1) in stereo. Domains are colored as in *A*. Strands in the S domain are numbered.

(MAD) method at 2.9 Å using data sets obtained from a single osmium derivative crystal (Table S1). The structure was further refined against 2 native data sets, form-1 (space group $C2, a = 152.7$ Å, $b = 52.9$ Å, $c = 76.2$ Å, and $\beta = 111.4°$) and form-2 (space group $C2, a = 138.6$ Å, $b = 51.4$ Å, $c = 76.4$ Å, and $\beta = 106.7°$) at 2.6-Å ($R = 0.243$; $R_{free} = 0.289$) and 2.8-Å ($R = 0.229$; $R_{free} = 0.280$) resolution, respectively (Table S1). Each crystal contained 1 ADAMTS13-DTCS molecule per asymmetric unit. The final model of the form-1 (form-2) crystal includes ADAMTS13 residues 299–322 (323), 331 (330)–458, and 466–682. Electron densities for carbohydrate moieties attached to 3 of the 4 potential *N*-linked (Asn-552, Asn-579, and Asn-614) and one *O*-linked (Ser-399) site were observed (*SI Text* and Fig. S1). Pro-379, Pro-414, Pro-475, and Pro-618, were in the *cis* conformation.

Overall Structure. The N-terminal portion of the C domain (residues 440–531, designated the C_A domain here) in ADAMTS13 has a fold structurally homologous to that of the C domain of ADAMs, despite the lack of sequence similarity. The D domain (residues 306–383) of ADAMTS13 also has a fold similar to the C domain of ADAMs, which is consistent with recent crystallographic studies (20–22). Therefore, ADAMTS13 possesses 2 homologous domains that belong to the ADAM_CR family (Pfam database entry: pfam08516). The remaining C-terminal portion of the C domain (residues 532–555) is highly conserved in amino acid sequence among ADAMTS family proteins (Fig. S2, here called the C_B domain). The domain architecture of ADAMTS13 is schematically represented in Fig. 1*A*.

The overall structure of ADAMTS13-DTCS resembles a distorted W-shape, in which 3 knobs, the D, C_A, and S domains, are connected by 2 elongated structural modules, T1 and C_B (Fig. 1*B*). The homologous D and C_A domains are separated and related by a pseudo-90° screw rotation with an ≈45-Å translation along T1 (Fig. 1*B*). T1 has a very similar structure to that of the prototypical TSR, TSR2, in TSP-1 (23) with an rmsd of 1.37 Å for the equivalent Cα atoms (Fig. S1) and an antiparallel 3-stranded fold. Although the C_B domain has no apparent secondary structure, it has a series of turns stabilized by a pair of disulfide bonds (Cys-532-Cys-548 and Cys-545-Cys-555) and forms a rod shape with its N and C termini ≈25 Å apart (Fig. 1*B*). The C_A and S domains, bridged by the C_B domain, make direct contact through the extended loop of the S domain (Fig. 1*B* and *SI Text*). The structures of ADAMTS13 obtained from the 2 crystal forms are essentially the same, with the exception of the relative orientations between the domains (*SI Text* and Fig. S3). The structural details of the D, C_A, and S domains are described in the following sections and T1 in *SI Text*.

Comparison of the D and C_A Domains. The D and C_A domains have only 17% identity in their amino acid sequences (Fig. S2); however, their tertiary structures are quite similar (Fig. 2 *A, B*, and *E*). They share an N-terminal α-helix, 2 pairs of double-stranded antiparallel β-sheets, and 3 disulfide bonds, constituting the core structure of these domains. The D domain has an additional disulfide bond (Cys-322-Cys-347) that is strictly conserved among the ADAM counterparts (22, 24). The 3 peripheral loops differ markedly in structure between D and C_A in
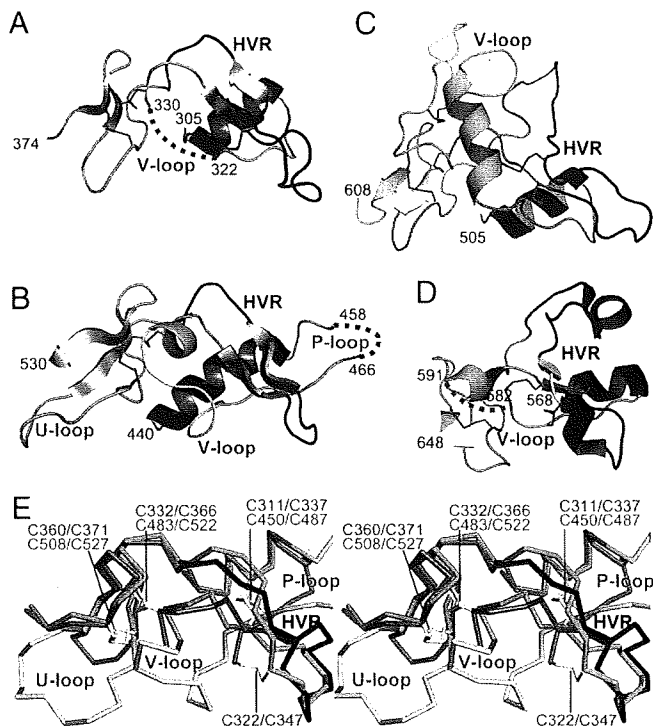
Akiyama et al.

Fig. 2. Comparison of the D and C_A domain structures. Ribbon representation of the D (A) and C_A (B) domains of ADAMTS13-DTCS, and the C domains of VAP1 (representative of canonical ADAMs, PDB 2ERO) (C) and ADAM10 (PDB 2AO7) (D). The conserved α-helix, β-strands, and disulfide bonds are shown in red, yellow, and orange, respectively. The V-loop and HVR are shown in gray and blue, respectively. Disordered regions in the crystals are shown as dotted lines. The numbers of the terminal amino acid residues are indicated. (E) Superimposition of the D (orange) and C_A (green) domains in stereo. Disulfide bonds are indicated in stick representations.

ADAMTS13 (Fig. 2E). The amino acid sequences of these loops are also quite different between D and C_A in ADAMTS13 and in other ADAMTS family members (Fig. S2).

The loop following the first α-helix of the C_A domain (residues 454–469) is 12 aa residues longer than that of the D domain, protrudes from the main body of C_A, and is disordered along the distal side (Fig. 2 B and E). We designated this C_A-specific loop as the protruding (P) loop. One region in the D domain (residues 323–329) is disordered (Fig. 2A), not only in the current ADAMTS13 structures, but also in other reported ADAMTS1 structures (20), although the corresponding region of C_A is clearly defined in electron density maps. We designated this loop the variable (V) loop because of its variability in both length and amino acid sequence (Fig. S2). Canonical ADAM family members have a helix-loop insertion of 26–30 aa residues in the V-loop (Fig. 2C), whereas the atypical ADAM10 does not, and its C domain is more similar to the D and C_A domains of ADAMTS13, except for the hypervariable region (HVR) (Fig. 2D) (22, 24). ADAMTS13 has an insertion of 6 residues (residues 512–517) just before the C-terminal β-sheet of C_A (Fig. 2 B and E), which is not found in other ADAMTS members (Fig. S2). We designated this loop the ADAMTS13-C_A-unique (U) loop. Each C domain contains a HVR that differs markedly among ADAMs and may play a central role in substrate recognition (22, 24). ADAMTS13 has shorter HVRs in both the D and the C_A domains than those present in the ADAMs (Fig. 2 A–D). These loops and HVRs were targeted for mutations (see below).

There is an Arg-498-Gly-499-Asp-500 integrin recognition sequence in the C_A domain. The side chain of Arg-498 is buried and

unavailable for protein–protein interactions, but the Asp-500 side chain is exposed toward the solvent.

Spacer Domain. The S domain is a long cysteineless segment and its primary structure shows no apparent homology to known structural motifs. The present study revealed that this region folds into a single globular domain with 10 β-strands in a jelly-roll topology, forming 2 antiparallel β-sheets that lie almost parallel to each other (Fig. 1B and Fig. S4A). The hydrophobic residues forming the core of the β-sandwich (Fig. S4B), a cluster of aromatic residues located on the concave outer surface of the smaller 4-stranded sheet (Fig. S4C), and proline and glycine residues in the loops, are highly conserved among ADAMTS proteins (Fig. S4D). Collectively, these findings suggest that ADAMTS proteins share the S domain architecture observed in ADAMTS13. In contrast, loops located at the distal side of the molecule are highly variable in both length and amino acid sequence among ADAMTS family members (Fig. S4D). The N and C termini of the S domain are in close proximity and thus the T2 following the S domain should be in close proximity to the C_A/S-domain junction but not the distal side of the S domain.

MDTCS Model. The reported crystal structures of the ADAMTS-MDs and our current ADAMTS13-DTCS structure enabled us to build an ADAMTS13-MDTCS model (Fig. 3A). The currently available ADAMTS-MD structures (20, 21) superimpose well on each other, except for subtle differences in the relative orientations of the M and D domains. We performed a functional assay using the ADAMTS13-MDTCS mutants F216E and A258C/K368C, which have modified interactions between the M and D domains. The results suggest that a stable association between the M and D domains is necessary for ADAMTS13 function (Fig. 3 B and D and SI Text).

VWF-Binding Exosites. We introduced mutations into ADAMTS13-MDTCS and measured the enzymatic activities of the mutants using the synthetic fluorogenic substrate FRETS-VWF73 (25). The results are summarized in Fig. 3 C and D.

In the current model, the D domain abuts the M domain catalytic site (Fig. 3B), suggesting that the surface of the D domain leading to the catalytic site functions as a VWF-binding exosite. Two mutants, 1 with a substitution in the HVR (D), R349D, and the other with 7 residues in the V-loop (D) replaced by a 4-residue linker, the ΔV-loop (D), exhibited diminished enzymatic activity (Fig. 3 C and D). The disordered V-loop (D) contains 4 charged residues, Arg-326, Glu-327, His-328, and Asp-330, which are suggested to lie in the vicinity of Arg-349 in the HVR (Fig. 3B). The cluster of these charged residues may collaboratively create an exosite (exosite-1). Charged amino acid-to-alanine substitutions revealed that Asp-1614, Glu-1615, and Lys-1617 in the VWF A2 domain act synergistically in ADAMTS13-mediated cleavage (26), suggesting that these charged residues in VWF are targets for exosite-1. Recently, Arg-349 was suggested to interact directly with VWF, most probably with Asp-1614 (27). Leu-350 and Val-352, which form a cluster of hydrophobic residues adjacent to the end of the catalytic cleft (Fig. 3B), also interact with VWF (27). This observation suggests that the hydrophobic cluster functions as a part of exosite-1.

The C_A domain has 3 surface loops. The ΔV-loop (C_A) mutant resulted in very low enzymatic activity (Fig. 3 C and D), suggesting that the V-loop (C_A) creates another exosite (exosite-2). A triple alanine substitution in the V-loop (C_A), H476A/S477A/Q478A, and a mutant at the N terminus of the HVR (C_A) adjacent to the V-loop (C_A), R488E, had significantly reduced activity (≈21%), suggesting that these hydrophilic or charged residues play a pivotal role in VWF recognition at exosite-2. The ΔU-loop and the F494Q/M496Q mutants showed reduced activity (≈40%) compared to the ΔP-loop mutant (≈53%). The
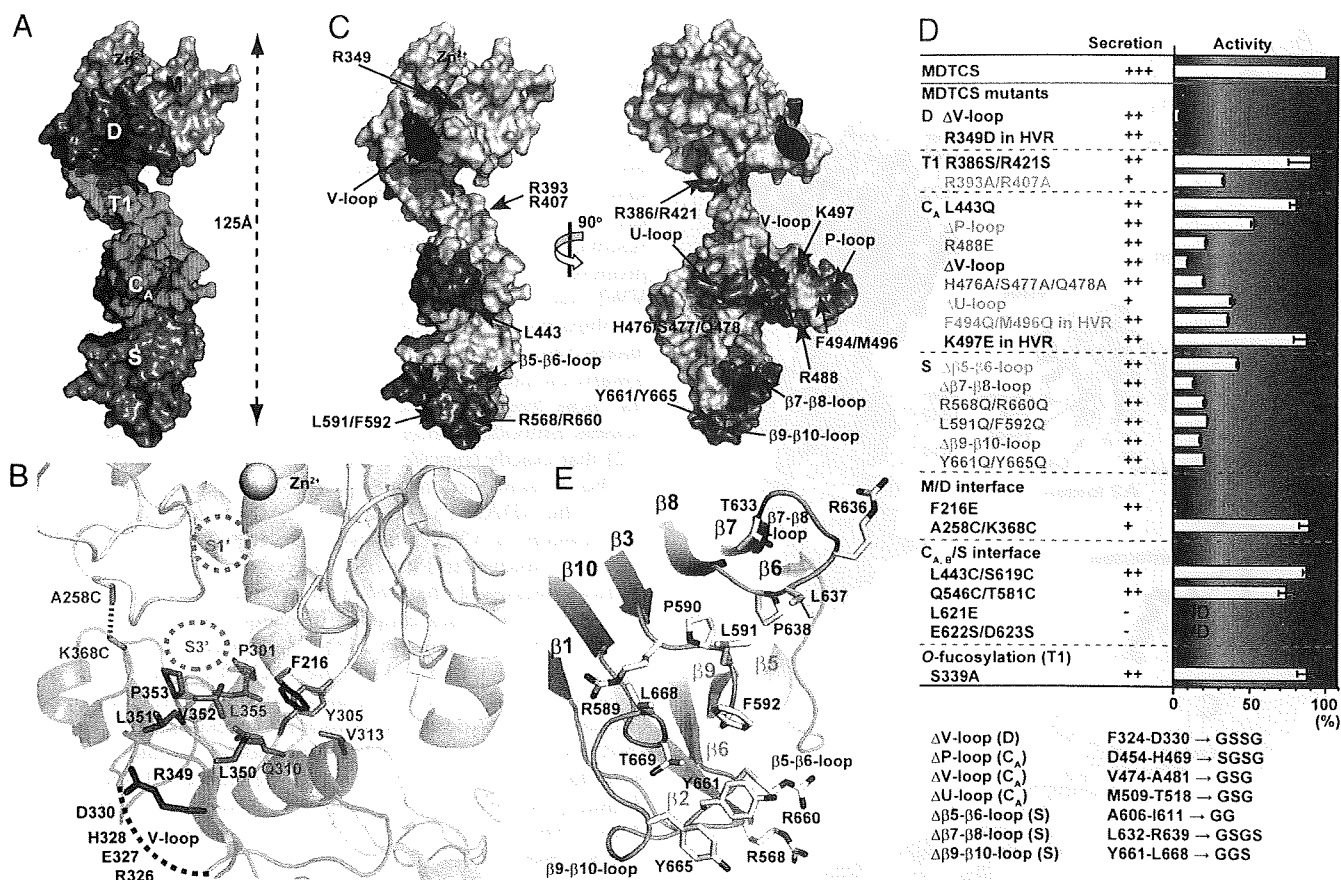
Fig. 3. A model of ADAMTS13-MDTCS and the residues affecting enzymatic activity. (*A*) Surface representation of the ADAMTS-MDTCS model. The M domain is shown in gray and the other domains are colored as in Fig. 1. The zinc ion is shown in yellow. (*B*) Close-up view of the interface between the M and D domains in the ADAMTS13-MDTCS model. Potential S1' and S3' substrate-binding sites, disordered V-loop (represented by a red dotted line), and the residues substituted by cysteine to form an interdomain disulfide bond (represented by a green dotted line) are indicated schematically. (*C*) The residues that affect ADAMTS13-MDTCS activity are indicated on the molecular surface, using a red-through-blue color-coding according to the results of the mutational assay shown in *D*. The molecule is viewed from 2 orthogonal directions. The V-loop of the D domain was disordered in the structures determined in this study and is represented by a red ellipsoid. (*D*) Summary of the mutational analysis, presenting the effects on secretion and enzymatic activity of the ADAMTS13-MDTCS mutants. Signs denote relative secretion level as follows: −, no detectable secretion; +, less than 30%; ++, 30~70%; +++, 70~100% of the secretion level of the wild type; ND, not determined. Relative enzymatic activities of the mutants are shown in the bar graph. The error bars indicate the range. (*E*) Close-up view of the hydrophobic cluster surrounded by arginine residues (exosite-3) in the S domain.

U-loop (C_A) and residues 494–496 flank the V-loop (C_A) and may contribute to exosite-2. In contrast, the P-loop is distant from the V-loop (C_A) and may contribute less to VWF binding. A mutation in the middle of the HVR (C_A), K497E, maintained enzymatic activity comparable to wild type, even though Lys-497 is the equivalent of Arg-349, the pivotal residue in exosite-1 in the homologous D domain.

The 3 distal loops in the S domain were replaced by short linkers and enzymatic activity in the mutants was assayed. The Δβ7-β8-loop and Δβ9-β10-loop mutants showed greatly reduced activity compared to the Δβ5-β6-loop mutant (Fig. 3 *C* and *D*). The β9-β10 loop contains 2 tyrosine residues, Tyr-661 and Tyr-665, which face the solvent. The Y661Q/Y665Q mutant was significantly less active (≈18%) than the wild type. These tyrosine residues and Leu-668 in the β9-β10 loop form a hydrophobic cluster together with residues in the neighboring β3-β4 and β7-β8 loops (Pro-590, Leu-591, Phe-592, Leu-637, and Pro-638) (Fig. 3*E*). Leu-591 and Phe-592 are located at the center of this hydrophobic cluster. The L591Q/F592Q mutant showed reduced activity (Fig. 3*D*). Four arginine residues surround the hydrophobic cluster (Fig. 3*E*). The R568Q/R660Q mutant was significantly less active than the wild type. Collectively, the hydrophobic cluster rimmed with arginine residues in the S domain may to be another VWF-binding exosite (exosite-3).

Mutations of residues (R386S/R421S and L443Q) located apart from the exosites and the O-linked fucosylation site (S339A) did not affect activity. The R393A/R407A mutation in T1 showed reduced activity (≈33%). Arg-407 is located at the bottom of a cleft formed between exosite-1 and exosite-2. This residue may also contribute to VWF binding.

Discussion

This study presents a structural determination of the ADAMTS13 DTCS domains, which constitute important functional part of the proteinase. The structure revealed that the residues important for stabilizing the DTCS core architecture are strictly conserved in all ADAMTS proteins. In contrast, peripheral loops within the D, C_A, and S domains were substantially different in both length and amino acid sequence among ADAMTSs, suggesting that these regions have specific functions that distinguish each ADAMTS member. By systematic mutagenesis, we identified 3 VWF-binding exosites in these loops (Fig. 3*C*). The exosites are highly conserved among ADAMTS13s from different species (Fig. S5). The 3 exosites were linearly aligned in the 3D structure, traversing the W-shaped ADAMTS13-DTCS molecule (Fig. 3*C*). This arrange-